Title

TOUGHREACT-Brine: Supplement to TOUGHREACT-V4.0-OMP User's Guide for Modeling Concentrated Solutions and Osmosis Using the Pitzer Ion-Interaction Model

Authors

Spycher, Nicolas
Zhang, Guoxiang
Sonnenthal, Eric
et al.

Publication Date

2022-12-23

Peer reviewed

LBNL-2001387

TOUGHREACT-Brine

Supplement to TOUGHREACT-V4.0-OMP User's Guide for Modeling Concentrated Solutions and Osmosis Using the Pitzer Ion-Interaction Model

Nicolas Spycher, Guoxiang Zhang, Eric Sonnenthal, and Sergi Molins

Energy Geosciences Division
Lawrence Berkeley National Laboratory

March 2021

ACKNOWLEDGMENTS

This work was supported by the Science & Technology Program of the Office of the Chief Scientist (OCS), Office of Civilian Radioactive Waste Management (OCRWM), U.S. Department of Energy (DOE), as well as by Assistant Secretary for Energy Efficiency and Renewable Energy, Geothermal Technologies Office, of the U.S. Department of Energy, under the U.S. Department of Energy Contract No. DE-AC02-05CH11231.

TABLE OF CONTENTS

TABLE OF FIGURES

1. INTRODUCTION

TOUGHREACT-Brine implements the Pitzer ion activity model (Pitzer, 1973) into V3.85-OMP and above, taking advantage of all code upgrades since the release of its predecessor version V1.21-Pitzer (Zhang et al., 2006), including Open-MP parallelization of the geochemical computations (Sonnenthal et al., 2018), bug fixes, and upgrades to simulate the osmotic flow of water and two-dimensional Poiseuille flow for applications to membrane desalination.

Contrarily to the previous standalone V1.21-Pizer version, this "Brine" version has been fully integrated into TOUGHREACT V4.00-OMP, which can be run with or without the Pitzer ion activity model option.

In this report, we present:

- The Pitzer ion-interaction theory and implemented model into TOUGREACT
- Input requirements for using the new Brine options
- Verification test cases
- Sample problems.

For the main code structure, features, overall solution methods, description of input/output files for parameters other than those specific to brine options the user is referred the latest TOUGHREACT User's Guide.

1.1 TOUGHREACT Versions and Pitzer Ion-Interaction Implementation

The first version of the nonisothermal reactive geochemical transport simulator, TOUGHREACT, was developed (Xu and Pruess, 1998 and 2001) by introducing a reactive geochemical model into the framework of the existing multiphase fluid and heat flow code TOUGH2 (Pruess, 1991). TOUGHREACT was further enhanced with the addition of (1) treatment of mineral-water-gas reactive transport under boiling conditions, (2) an improved HKF activity model for aqueous species, (3) gas-species diffusion coefficients calculated as a function of pressure, temperature, and molecular properties, (4) mineral reactive surface area formulations for fractured and porous media, and (5) porosity, permeability, and capillary pressure changes owing to mineral precipitation/dissolution (Sonnenthal and Spycher, 2001; Spycher et al., 2003; Sonnenthal et al., 2005).

The only previously released TOUGHREACT version incorporating the Pitzer ion-interaction model (Zhang et al., 2006) was developed based on version V1.21 (Xu et al., 2004). The main extensions included (1) the implementation of the Pitzer ion-interaction model (Pitzer and Mayorga, 1973; Pitzer, 1991) for ionic activity calculation of solutions over a broad range of concentrations and (2) the coupling of the vapor-pressure-lowering effect of salinity to phase partitioning. These options were streamlined for computing efficiency and, together with a new capability to simulate osmotic transport of water, were ported into TOUGHREACT V4.0-OMP as permanent optional features of this and future code versions.

The mathematical and numerical description of the nonidealities of concentrated aqueous solutions involves many nonlinear ion-interaction terms and various interaction parameter sets (e.g., Pitzer

and Mayorga, 1973; Pitzer, 1991; Harvie et al., 1984; Wolery et al., 2004). Thus, numerically modeling these solutions can be computationally intensive. For this reason, the implementation of the Pizer ion activity model in the present code version was reworked (e.g., considering only key partial derivatives in the Jacobian matrix) and implemented in a way that essentially does not affect computing performance when the Pitzer option is not selected. Because of these improvements and the parallelization of the code since early V1.21, the Pitzer option with this TOUGHREACT version is computationally orders of magnitude faster than with its predecessor V1.21-Pitzer.

1.2 Capabilities and thermodynamic data

Concentrated aqueous solutions are significantly different from dilute solutions not only in terms of geochemical behavior (e.g., water activity and ionic activity coefficients far from unity), but also in terms of flow and transport because of elevated density and viscosity. However, the Pitzer ion-interaction model implemented in TOUGHREACT is currently used only for the calculation of water activity and activity coefficients of dissolved species, and not for other physical properties such as density and viscosity. These properties are computed separately in the TOUGH2 equation of state (EOS) selected for implementation with TOUGRHEACT. Currently the most appropriate equation of state to simulate brine flow with TOUGHREACT is EOS7.

The Pitzer formalism was implemented into TOUGHREACT using the Harvie-Moller-Weare (HMW) formulation (Harvie et al. 1984). The HMW formulation was developed from Pitzer's ion-interaction theoretical model and is equivalent to Pitzer's original model (Pitzer, 1973; and Pitzer and Mayorga, 1973). The only difference is in the definition of interaction terms, interaction coefficients, and mathematical expressions (Rard and Wijesinghe, 2003). The HMW formulation is often preferred to Pitzer's original formulation because it is more convenient for numerical implementation. Also, parameters for the HMW formulation are often more readily available from the literature than parameters for Pitzer's original formulation.

The HMW formulation implemented in TOUGHREACT is documented in APPENDIX A. The implementation of the Pitzer model allows TOUGHREACT to deal with concentrated solutions, with limits on ionic strength, temperature, and pressure depending on the types and validity range of ion-interaction parameters in the thermodynamic database. Pitzer thermodynamic databases formatted for use with this code version include (but are not limited to):

- A conversion of the EQ3/6 *data0.ypf* Pitzer database (after Wolery et al., 2004; see also Alai et al., 2005), suitable for ionic strengths up to ~40 molal for some systems and temperatures around 150°C at solution vapor saturation pressures

- A conversion of the PHREEQC v3.06 *Pitzer.dat* database (Plummer et al., 1988), suitable primarily for low-temperature applications

Upgrades of these databases and/or other databases may be included in the distribution package. These thermodynamic databases are provided "as-is", and users should refer to the cited references to determine whether these are suitable, or not, for their particular application. Also, before using the Pitzer ion interaction model with TOUGHREACT, it is imperative that users be familiar with the Pitzer formalism, potential pitfalls when mixing thermodynamic data from different sources,

and particularly the potential for "double-counting" ion association effects when including aqueous complexes in simulations.

The Pitzer model in TOUGHREACT accounts for interaction terms of cation-anion, cation-neutral, anion-neutral, cation-cation, anion-anion, cation-anion-anion, cation-cation-anion, neutral-cation-anion, neutral-cation-cation and neutral-anion-anion combinations (Appendix A). When dealing with reactive transport problems for a given solution, with a pre-estimated ionic strength range, simplifications may be made by neglecting some of these interaction terms to save computational time without losing significant accuracy (Section A.2).

Water activity is a function of salinity and (by convention) is defined with a unit activity for pure water. As salinity increases, the water activity decreases, and thus affects the water vapor pressure owing to the equilibrium between the solution and its vapor. The lowered vapor pressure can significantly alter vapor flow patterns in a particular system. The lowered vapor pressure also implies elevation of the boiling point, which then alters the temperature field and liquid saturation pattern when a concentrated solution is heated. In this version of TOUGHREACT, this effect of vapor pressure lowering with increasing salinity is taken into account such that subsequent effects can be properly simulated.

2 IMPLEMENTED PROCESS MODELS

2.1 Pitzer Ion-Interaction Model

In a given aqueous solution, the thermodynamic activity of a dissolved species is a function of the solution excess free energy, which is, in turn, a function of temperature, pressure, chemical composition of the solution, and the thermodynamic properties of the solutes. In the solution, ions with opposite signs attract and interact with each other. Some of the ions with opposite signs are bound by their ionic charges, leading to aqueous complexes. Meanwhile, some of the ions tend to depart from each other, leading to the existence of free ions in the solution. The ratio of the bounded ions and free ions is a constant under given composition, temperature and pressure conditions, and is quantified in the thermodynamic equilibrium theory. The thermodynamic activity of any ion in the attraction-repulsion processes is determined by (1) the abundance of that ion in the solution and (2) the nonideal behavior of the ion in solution. The abundance of that ion is the concentration of the free ion. Nonideality, evaluated using an ionic activity coefficient, is a complex function of temperature, pressure, and concentrations.

Dilute solutions (typically with ionic strength, I, < 0.1 molal) are considered quasi-ideal solutions. The nonidealities of such solutions are minor and are mainly attributed to long-distance ionic interactions, which can be quantified using ionic strength. The activity coefficients of species in those solutions can be calculated with simple models, such as the Debye-Hückel model and its variations, in which only solution ionic strength and ionic properties are accounted for in the calculation. The effects of interactions among individual ions are either neglected or lumped into general extensions of the Debye-Hückel model.

The nonidealities in concentrated solutions (ionic strength I > 0.1 molal, and especially I > 1 molal) are significant because the distances between ions are much shorter than those in dilute solutions.

Most ions in such solutions are neither completely dissociated nor tightly associated, because of the short distance and strong interactions among ions in the solutions. Instead, ions engage in attraction-repulsion interactions with other ions. Ionic activity is mainly attributed to such interactions. Activity models that apply to dilute solutions, such as the Debye-Hückel model and its extensions, are no longer suitable in such concentrated solutions. To calculate ionic activities, one needs to consider interactions among different individual ions.

A quantitative description of how ion interactions affect the ionic activities in concentrated aqueous solutions is given in Pitzer (1973). Pitzer's model formulates the ionic activity as a function of each individual ionic interaction, i.e., the interactions among each cation-anion pair, cation-cation pair, anion-anion pair, and various ternary ionic combinations and other possible interactions. Like-sign pairs and ternary ionic combinations result from multiple salt contributions (also referred to as mixing terms). The Pitzer model evaluates the ionic activity of a solution as a function of solution ionic strength (long-distance interaction), interaction terms (short-distance interaction), temperature, and pressure. The model formulation consists of several virial equations, sometimes called specific interaction equations, Pitzer equations, or phenomenological equations. These equations can adequately express the thermodynamic properties of the concentrated solution over a wide range of concentrations and temperatures (Clegg and Whitfield, 1991). The Pitzer model is based on a virial expansion (Pitzer, 1973) that essentially reduces to the Debye-Hückel equation at low ionic strength (Pitzer, 1991). This virial expansion involves summations over all possible binary and ternary short-range interaction terms, as well as mixing terms. A generally accepted form of the Pitzer model was formulated by Harvie et al. (1984) and referred to as the HMW formulation. This formulation has been adopted in several computer codes, such as PHRQPITZ (Plummer et al., 1988), GMIN (Felmy, 1995), and BIO-CORE$^{2D©}$ (Zhang, 2001; Zhang et al., 2005). In EQ3/6, Wolery and Daveler (1992) and Wolery and Jarek (2003) use Pitzer's original formulation but also make use of interaction parameters for the HMW formulation by mapping these parameters into the formulation implemented in the code. The HMW formulation was implemented in TOUGHREACT, with details given in Appendix A.

2.2 Vapor-Pressure Lowering

2.2.1 Salt Effects

Vapor-pressure lowering caused by dissolved salts was implemented in TOUGHREACT for multiphase flow simulation, using the water activity computed with the Pitzer ion-interaction model (Section 2.1). For equilibrium between water and H_2O vapor (i.e., for the reaction $H_2O_{(l)} \Leftrightarrow H_2O_{(g)}$), equating the chemical potentials of both phases yields:

$$\begin{aligned} \mu^0_v - \mu^0_w = {} & RT \ln(f_v / f^0_v) - RT \ln(f_w / f^0_w) \\ & = RT \ln(f_v / a_w) = RT \ln(K) \end{aligned} \tag{2.1}$$

where subscripts w and v stand for liquid water and H_2O gas, respectively, μ^0 stands for the reference chemical potential, f is fugacity, a is activity (defined as f/f^0, with f^0 being the fugacity in the reference state), K is the thermodynamic equilibrium constant, R is the gas constant, and T is absolute temperature. The reference (standard) state of H_2O gas is taken as unit fugacity or the pure gas at 1 bar pressure and all temperatures (i.e., f^0_v = 1 bar in Equation 2.1), whereas that of

liquid water is taken as unit activity of pure water at all temperatures and pressures (i.e., $f_w / f^0_w = a_w = 1$ in Equation 2.1). Using this convention yields:

$$f_v = a_w K \tag{2.2}$$

In our case, at low pressure (atmospheric), fugacity is approximated by pressure, such that $f_v \cong P_v$, the pressure of H_2O gas (the actual vapor pressure). When the system is pure, $a_w = 1$ and Equation (2.2) yields $f_v = K \cong P^0_{sat}$, the vapor pressure of pure water. Accordingly, the vapor pressure of the solution can be computed as:

$$P_v = a_w P^0_{sat} \tag{2.3}$$

Equation (2.3) is used in the coupling of chemistry and flow calculations, such that the effect of salts on vapor pressure is taken into account in the multiphase flow computations. From Equation (2.3), it is also apparent that if relative humidity, Rh, is defined as the ratio of the actual vapor pressure over that of pure water, then we have:

$$Rh = a_w \tag{2.4}$$

2.2.2 Salt and Capillary Pressure Effects

The effect of capillary suction on vapor pressure is already implemented in module EOS4 using a dimensionless modification factor, F_v, derived from the Kelvin equation and defined as:

$$F_v = e^{\frac{P_c V_l}{RT}} \tag{2.5}$$

where P_c is the capillary pressure (Pa, negative), V_l is the molar volume of pure water (m^3/mol) at absolute temperature T (in K) and at saturation pressure of pure water, and R is the universal gas constant (Pa m^3 mol^{-1} K^{-1}). This factor is used to lower the water vapor pressure (P^0_{sat}, with no capillary suction) as follows:

$$P_v = F_v P^0_{sat} \tag{2.6}$$

As mentioned above, the standard state for liquid water-activity calculations in TOUGHREACT is unit activity at any temperature and pressure (including negative pressures reflecting capillarity). Using this convention, the effect of capillarity on water activity should be accounted for by the effect of pressure on K in Equation (2.2), without recourse to a separate vapor-pressure-lowering factor, F_v (i.e., by applying a Poynting correction, which is essentially identical to F_v, directly to K in Equation 2.2). However, the water/vapor equilibrium in TOUGHREACT is handled through steam tables for pure water implemented in the TOUGH2 routines of this code, and not through the intermediary of Equation (2.2). Therefore, Equations (2.3) and (2.4) are valid only when the capillary pressure is zero. To consider the effect of capillary pressure, when using EOS4, these equations have been replaced by, respectively,

$$P_v = a_w F_v P^0_{sat} \tag{2.7}$$

and

$$Rh = a_w \times F_v \tag{2.8}$$

2.2.3 Water-Vapor Local Equilibrium

In a groundwater flow system, under typical flow conditions, local equilibrium (water-vapor steady-state system) is generally reached because the groundwater and vapor fluxes are small relative to the rate of local water-vapor transfer. This local equilibrium is the basic assumption of the TOUGH2 and TOUGHREACT code for multiphase flow calculations. Local water-vapor equilibrium is always imposed during each flow time step. Thus, the model yields the equilibrium state at each successive time step. Disequilibrium over a large spatial scale is captured by the spatial discretization, with vapor flow being driven by the vapor-pressure gradient from one model grid block to the next. Because water-vapor equilibrium is assumed in each grid block, the air relative humidity is always 1 if pure liquid water is present and if effects of capillary pressure are neglected.

2.2.4 Modified Equation of State (EOS) Modules

The following EOS modules of TOUGHREACT were modified to account for salinity-driven vapor-pressure-lowering effects:

- EOS1, EOS2, EOS3, EOS5, EOS7, EOS8: vapor-pressure lowering by salinity only, Equations (2.3) and (2.4)
- EOS4: vapor-pressure lowering by capillary pressure and salinity, Equations (2.7) and (2.8)

2.3 Osmotic Transport of Water

This version of TOUGHREACT allows for modeling the osmotic transport of water, such as through forward and reverse osmosis membranes, following its chemical potential gradient:

$$J = \frac{D}{RT} C \, d\mu / dx \tag{2.9}$$

where J represents flux, D is the diffusion coefficient, R is the gas constant, T is temperature, C is concentration, x is distance, and μ is the water chemical potential defined as:

$$\mu = RT \, lna + \int_{P0}^{P} V dP \tag{2.10}$$

In the above equation, a stands for the water activity, computed with the Pitzer (or HKF) model; the integral of molar volume V from reference pressure P^0 to applied pressure P is approximated by

$$\int_{P0}^{P} V dP \approx \bar{V}(P - \mathrm{P}^0) \tag{2.11}$$

using the average molar volume of water $\bar{V}$ in the pressure interval P^0 to P (18 cm^3/mol for typical applications). Defining the water activity $a = \gamma C$, with γ being the water activity coefficient, Equation (2.10) can then be re-expressed as:

$$\mu = RT \ln(\gamma C \exp^{\bar{V}(P-P^0)}) = RT \ln(a') \tag{2.12}$$

with the term a' now encompassing the effect of pressure. Substituting Equation 2.12 into 2.9 and assuming a constant temperature yields

$$J = \frac{D}{RT} C \frac{d[RT \ln(a')]}{dx} = D \frac{C}{a'} \frac{da'}{dx} \tag{2.13}$$

thus

$$J = \frac{D}{\gamma \exp^{\frac{\bar{V}}{RT}(P-P^0)}} \frac{da'}{dx} = D' \frac{da'}{dx} \tag{2.14}$$

This equation takes the form of the Fick's Law implemented in TOUGHREACT for the diffusion of solute species, and is used directly for water after recasting D and a as D' and a', respectively. The water diffusion coefficient in the membrane is typically about 2×10^{-10} m^2/s (Geise et al. 2016, their Figure 16). The water self-diffusion coefficient outside the membrane is, for the time being, fixed internally at 2.3×10^{-9} m^2/s at 25°C (Mills, 1973).

For the case of thin membranes, to avoid the necessity to discretize space down to the membrane thickness (typically 200 nm), an option is available to approximate the water flux through the membrane as (Wijmans and Baker, 1995):

$$J = A(\Delta P - \Delta \Pi) \tag{2.15}$$

where A is the membrane permeance (also referred to as permittivity or permeability) and ΔP and $\Delta \Pi$ are the differences in pressure and osmotic pressure, respectively, between both sides of the membrane. The permeance is entered in file *solute.inp* (in units of [L m^{-2} s^{-1} bar^{-1}]) and lumps the membrane thickness and diffusive properties as

$$A = \frac{D\bar{V}}{dRT} \tag{2.16}$$

where d (in [m]) is the active membrane thickness, $\bar{V} = 18 \times 10^{-3}$ [L/mol] is the water average molar volume in the pressure range of interest, and D (in [m^2/s]) is the water diffusion coefficient in the membrane. With these units the gas constant R is 8.314×10^{-5} m^{3}bar K^{-1} mol^{-1}, and temperature T is in [K].

It should be noted that the permeance is sometimes expressed in units of [mol m^{-2} s^{-1} bar^{-1}], in which case this parameter is defined as

$$A' = \frac{D\bar{V}C}{dRT} \tag{2.17}$$

where C is the water concentration in [mol/L] (e.g., Wijmans and Baker,1995, below their Equation 37) (C = 55.507 [mol/kg_{H2O}] × density [kg_{sln}/L] × 1/(1+kg_{salts}) [kg_{H2O}/kg_{sln}]).

The osmotic pressure is defined (and calculated) in TOUGHREACT from the water activity, a, as

$$\Pi = -\frac{RT\,ln(a)}{\bar{V}} \tag{2.18}$$

with variables and their values as previously defined. This equation is obtained by equating the chemical potential of pure water with that of saline water, with reference pressure at 1 bar.

In TOUGHREACT, the activity of water is computed from the osmotic coefficient, ∅, which when the Pitzer option is enabled is computed using the ion interaction parameters that are read in the thermodynamic database (Equation A2):

$$\ln(a) = -\frac{M_w}{1000}\left(\sum_{i=1}^{N} m_i\right)\varnothing = -\frac{(1-x_w)}{x_w}\varnothing \tag{2.19}$$

In this equation M_w is the water molecular weight (18.01 g/mol), m_i are the molalities of all (N) dissolved species i =*1 to N*, and x_w is the water mole fraction. This definition of ∅ is based on a molality scale, and should not be confused with the definition of the osmotic coefficient using a mole-fraction scale (in this case, $\ln(a) = \varnothing' \ln(x_w)$, see Denbigh 1981).

2.4 Poiseuille Flow for Parallel Plates

With the modeling of desalination membranes in mind, a capability was added to TOUGHREACT to mimic Poiseuille flow in the case of 2D-flow through a channel delimited by two parallel plates. When this option is enabled, flow velocities are scaled such that they decrease to zero at modeled surfaces following a Poiseuille distribution, according to the equation:

$$v / v_{avg} = -6\left[\left(\frac{y}{d}\right)^2 - \left(\frac{y}{d}\right)\right] \tag{2.20}$$

where v is the scaled fluid velocity as a function of distance y from the channel surface, v_{avg} is the average fluid velocity in the channel, y is the distance from the modeled surface, and d is the channel aperture (Figure 2-1).

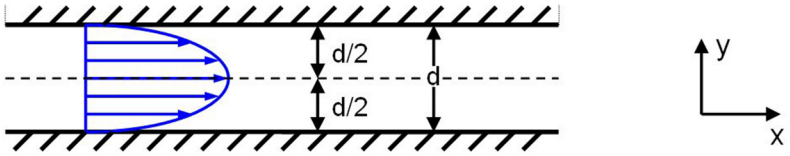

Figure 2-1. Schematic of Poiseuille flow velocity distribution (arrows) in a channel of aperture d, represented by Equation (2.20).

3 INPUT FILE UPDATES

3.1 Updates in Flow Inputs (*flow.inp* file)

The only updates in file *flow.inp* for using the Pitzer ion-interaction model are in the MOPR parameters, which are input under the keyword "REACT". Parameters MOPR(21)-MOPR(25) are new control parameters for the Pizter ion-interaction model and osmosis as described below.

REACT input block

Variable: MOPR
Format: 30I1

MOPR(21) This flag is used to turn the Pitzer activity coefficient model on or off.
=0: Default HKF extended Debye-Hückel activity coefficient model (same model as in previous code versions).
>0: Turns on the Pitzer activity coefficient model. Care must be taken to use a Pitzer thermodynamic database consistent with this option (with input file name specified in file *solute.inp*)

When using this option, users should make sure to use an appropriate Pitzer thermodynamic database, with ion-interaction parameters located at the bottom of the database, and making sure that secondary species (ion pairs) accounted for by the Pitzer ion-interaction parameters are not "double-counted" by secondary species. See Section 3.3 for important considerations regarding this matter.

MOPR(22) Only active when MOPR(21) > 0
=0: Pitzer model without simplifications
=1: nca terms omitted (only ca, cc, aa, cca, and caa terms)
=2: nca, cca, and caa terms omitted (only ca, cc, and aa terms)
=3: nca, cca, caa, cc, and aa terms omitted (only ca terms)
(n, c, and a stand for neutral species, cations, and anions, respectively)

MOPR(23) Only active when MOPR(21) > 0
=0: Consider ionic strength in mixing terms
=1: Ignore ionic strength in mixing terms

Default values for MOPR(22) and MOPR(23) are 0. It is the responsibility of the user to ensure that the selected level of simplification is appropriate for the intended use (see Appendix A, Section A.2). "Rule of thumb" values for MOPR(22) and MOPR(23) are as follows:

For I < 5 m	MOPR (22) = 3 and MOPR (23) = 1
For I = 5–10 m	MOPR (22) = 2 and MOPR (23) = 0
For I > 10 m	MOPR (22) = 1 or 0, and MOPR (23) =0

MOPR(24) This flag is used to enable water vapor-pressure lowering due to dissolved salts with either the HKF or Pitzer models; Equations (2.3) and (2.7). This option is not to be confused with vapor-pressure lowering due to capillary pressure, which is enabled when using the EOS4 module; in this case, the salt effect on vapor pressure is added to the capillary pressure effect.

= 0: vapor-pressure lowering due to salts is neglected.
= 1: vapor-pressure lowering due to salts is enabled.

Default value is 0. Note that vapor-pressure lowering due to dissolved salts can become quite large at high salinities. To determine whether to consider or neglect this effect, the vapor-pressure lowering factor can be approximated as the water mole fraction in solution (on the basis of fully ionized salts).

MOPR(25) =0: Default, no effect
=1: Turns on water transport by diffusion following its chemical potential gradient (Equation 2.9)
>1: turns on transport of water by diffusion according to its chemical potential, but not coupled with flow (not mass balanced – used for debugging or to look at the concentrative effect of RO without inducing flow)
>0: Diffusion coefficients followed by activation energy values for transport of primary species within modeled membranes are read from the thermodynamic database, following the molecular weight entry, for grid blocks with material name **ROmem** or for connections between grid blocks given material names **perm1** and **feed1** (see below).

ROCKS input block

MAT **ROmem** New specific material name to define a membrane. Grid blocks with this rock type will be assigned the diffusion coefficients that are read in the thermodynamic database. This material is used to simulate a membrane discretized with specific grid blocks given this material name.

perm1 and **feed1** New specific material names that automatically (and internally) set ISOT=10 for connections with adjacent materials **feed1** and **perm1**, for use with the *permean* option (see below and Equation 2.15).

The connection between such grid blocks is treated as an impermeable membrane allowing only diffusion. This option is typically preferred to simulate reverse osmosis because it does not require spatial discretization of the membrane (i.e., the membrane is treated as a connection)

CONNE input block

ISOT If ISOT = 10 and a non-zero variable *permean* is defined in input file *solute.inp*, the permeance approximation (Equation 2.15) will be used to compute water diffusion across this connection, such that a membrane can be modeled without having to be discretized (i.e., the membrane is actually just a connection). **Note:** The hydraulic permeability across this connection is set to zero (no advective transport), and the diffusion coefficients for species other than water applying to this connection are read from the thermodynamic database. Also, liquid saturation and porosity in the diffusion terms for this connection are internally set to 1. **Note:** as mentioned above, ISOT is automatically (and internally) set to 10 for connections with adjacent material names **feed1** and **perm1.**

New input block: POISEUILLE

POISEU(ILLE) Format A5
x_{start}, y_{start}, x_{end}, y_{end}, d Free format

Starting <x_{start},y_{start}> and ending <x_{end}, y_{end}> coordinates of line defining the surface (in 2 dimensions) on which velocity is scaled down to zero
d is the modeled channel full aperture in the positive y direction (see Figure 2-1)
Up to 4 different lines can be entered (for 4 different surfaces)

In the MESH file, the scaling is applied to those grid blocks flagged with new parameter *ipois* > 0, entered on each record of the ELEME file (or block) following the grid block coordinate. The value of ipois (1 to 4) must correspond to the order of the record (line coordinates) entered in the POISEULLE block (1 for first line, 2 for second line etc.)

Important notes:

- This option is intended only for a structured orthogonal 2D <X;Y> mesh with flow in the X direction (with initial velocity $v_y = 0$)
- Because this option is intended (and only valid) for 1-dimensional flow in X, the values of y_{start} and y_{end} should be the same, and typically be the same or close to the y coordinate of the grid block interface representing the membrane surface.
- This option is currently implemented in the code by multiplying the channel permeability values by the coefficients given by Equation 2.20. This results in velocities that are scaled according to *d* (see Figure 2-1), with the constraint that the average velocity (across *d*) equals the (plug) flow velocity returned from the flow EOS module.

- If injection is turned on (GENER), one injecting grid block per row of grid blocks in Y must be entered in the GENER input block, AND the generation rate should be weight-averaged by the increment Δy of each row of grid blocks. This is very important! Otherwise, this option may not yield the proper mass balance of solutes and/or create flow instabilities at the modeled system inlet.
- The scaled velocities output in the flow vector file can be used to check that the scaling is working properly.

3.2 Updates in Transport Inputs (*solute.inp* file)

Record_3. Options for Reactive Geochemical Transport (2)

Variable: SL1MIN, RCOUR, STIMAX, CNFACT, AWMIN
Format: 5E10.4

The first four parameters are unchanged from previous versions (Sonennthal et al., 2018).

AWMIN is an optional parameter. It is the water activity lowest limit allowed in simulations. If zero, or not entered, it is set by default to 0.1. Water activity values below this limit are reset to AWMIN during chemical iterations to avoid convergence problems at very low water activity values.

Record_5. Weighting parameters, diffusion coefficients, and reverse osmosis membrane parameters

Variable: WTIME, WUPC, DIFUN, DIFUNG, permean, disper, exp_pporo
Format: 7F

Three new parameters permean, disper, and exp_pporo can be entered on this record (optional). Other parameters are unchanged from previous versions (Sonnenthal et al., 2018). These new parameters are used only to model desalination membranes as described below:

permean Optional membrane water permeance **input in units of L/m^2/s/bar** This parameter is used only when adjacent grid blocks are given material names *feed1* and *perm1* (or ISOT for connections is set to 10). In this case, the membrane is not explicitly discretized and water diffusion through the membrane is represented by a connection with a given permeance (see Section 3.1). If permean > 0.0, the water flux J (by diffusion) between these grid blocks is computed using Equation 2.15.

disper Optional dispersion coefficient in units of meter (m) to approximate mixing/dispersion in the feed channel. If non-zero, a term equal to v×disper is added to the water diffusion coefficient, where v is the water flow velocity within the feed channel (along the membrane).

exp_pporo Optional (and preliminary/experimental) exponent << 1 to limit the flux of water through the modeled membrane when mineral precipitation occurs in the feed channel. If non-zero, the water diffusive flux through the membrane is multiplied by a factor $F = (\theta/\theta_0)^{exp\_pporo}$, where the ratio θ/θ_0 represents the ratio of current to initial porosity.

3.3 Pitzer Thermodynamic Database

Several thermodynamic databases are provided in the software distribution package (See Section 1.2). Their input format is identical to other TOUGHREACT databases, except that parameters to compute Pitzer ion-interaction parameters as a function of temperature are introduced at the bottom of each database. The input format for these parameters is the same as the format adopted in EQ3/6 (Wolery et al., 2004) except that the temperature functions have been expanded with two additional terms for compatibility with a range of other databases, as further described below. The dependency of the Pitzer parameters on pressure is not currently considered because the effect of pressure is much less significant than the effect of temperature within the current temperature range considered.

The interpolation and extrapolation equations, as a function of temperature, for various thermodynamic properties of aqueous solutions, for binary and ternary systems, and for multiple-component mixtures within the Pitzer formulation have been reported in many papers (Harvie et al., 1984; Pabalan and Pitzer, 1989; Harvie et al., 1987; Moller, 1988; Greenberg and Moller, 1989; Monnin, 1989 and 1994; Pitzer, 1991; Weber et al., 1999). These authors utilized a variety of activity data, enthalpy data, and heat capacities to construct comprehensive equations over the temperature range of 0 to 250°C. For example, Pabalan and Pitzer (1989) fitted their experimental results with equations using more than twenty adjustable parameters. Moller (1988) and Greenberg and Moller (1989) used an equation with ten adjustable parameters to describe the temperature-dependent parameters.

In this version of TOUGHREACT, the following algebraic equation is implemented:

$$P(T) = a_1 + a_2(\frac{1}{T} - \frac{1}{T_0}) + a_3\, ln(\frac{T}{T_0}) + a_4(T - T_0) + a_5(T^2 - T_0^2) + a_6(\frac{1}{T^2} - \frac{1}{T_0^2}) \qquad (3.1)$$

where $P(T)$ represents Pitzer parameters $\beta^{(o)}$, $\beta^{(1)}$, $\beta^{(2)}$, α, Φ, Ψ, and C_{MX}^{Φ} at temperature T (absolute temperature); and T_0 is the reference temperature (298.15 K used in the database). It should be noted that the temperature range of Pitzer ion interaction parameters may be different in different databases (see Section 1.2).

When applying the Pitzer ion-interaction model, the effect of ion pairing and aqueous complexation is generally taken into account by the ion-interaction parameters. Therefore, much care must be taken to avoid "double counting" by including in simulations only those secondary species that were specifically included in the fits of experimental data used to determine the ion-interaction parameters used in the simulation.

4 VERIFICATION TESTS WITH SINGLE SALTS

4.1 Verification Test 1: Calculation of the Mean Activity Coefficients and Osmotic Coefficients of Solutions up to 9 m *CaCl₂* at Temperatures of 80°C

In this test, we calculate the mean activity coefficients of *CaCl₂* and the osmotic coefficient of solutions up to 9 molal *CaCl₂* at a temperature of 80°C using the EOS3 module. The calculated mean *CaCl₂* activity and osmotic coefficients of the solution are then compared with the data from Ananthaswarmy and Atkinson (1985). These authors collected measured thermodynamic properties of *CaCl₂* solutions at various temperatures and concentrations (e.g., activity coefficients, osmotic coefficients, apparent mole heat capacity, apparent model enthalpies, differential heat of dilution of *CaCl₂* in temperature range 0–100ºC, and water-vapor-pressure data), fitted a data set to appropriate Pitzer equations as modified for *CaCl₂* by Rogers (Rogers 1981), and presented the mean activity coefficients, osmotic coefficients for *CaCl₂* solutions at various temperature and various molalities as reference data of *CaCl₂* solutions. Note that comparisons of mean activity coefficients, rather than mean activities, are appropriate here, because no significant amounts of *Ca* or *Cl* secondary species are calculated to form.

The mean activity coefficient of *CaCl₂* is calculated as:

$$\ln(\gamma_{CaCl_2}) = \frac{2\ln(\gamma_{Cl})+\ln(\gamma_{Ca})}{3} \tag{4.1}$$

where γ_{CaCl_2} is the mean activity coefficient of *CaCl₂*, γ_{Ca} is the activity coefficient of Ca^{+2}, and γ_{Cl} is the activity coefficient of Cl^{-}.

The osmotic coefficient is calculated as:

$$\emptyset = -\frac{\ln(a_w)*1000}{W_w \sum_i m_i} = -\ln(a_w)\frac{x_w}{x_w-1} \tag{4.2}$$

where $\emptyset$ is the solution osmotic coefficient, a_w and x_w are the water activity (calculated with TOUGHREACT and read from file *chdump.out*) and mole fraction, respectively, W_w is the water molecular weight, and m_i is the molality of each aqueous species *i* in the solution. The comparison between the calculation and the reference data is shown in Figure 4-1.

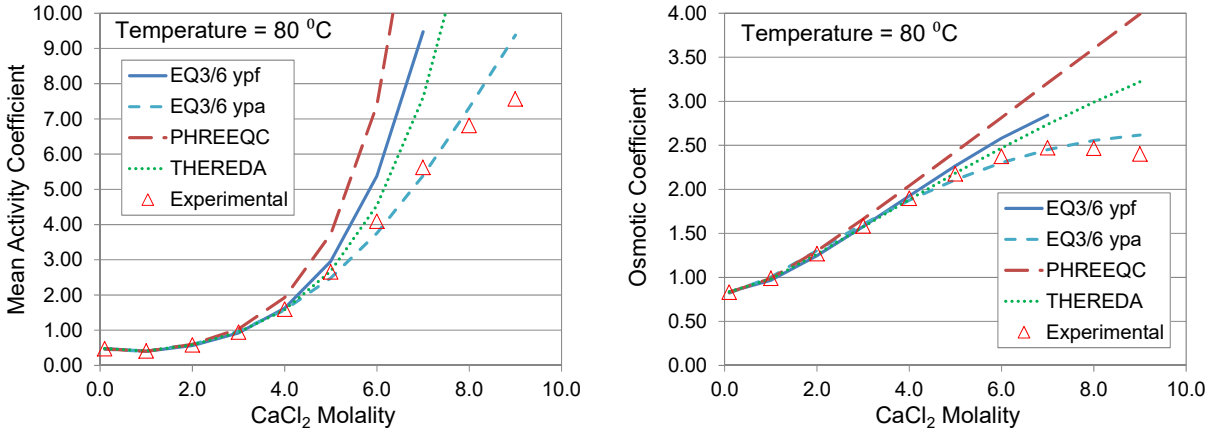

Figure 4-1. Comparison of the TOUGHREACT-calculated (solid lines) mean activity coefficient of $CaCl_2$ *and osmotic coefficient of the* $CaCl_2$ *solution to literature data (symbols) from Ananthaswarmy and Atkinson (1985), using different input thermodynamic databases.*

Note that Ananthaswarmy and Atkinson (1985) report that at high ionic strength, their data are questionable. This may be a result of a possible solid phase formed in the solution at concentrations reaching saturation of the salt. This would explain the larger discrepancies between their data and the TOUGHREACT results at high *CaCl2* concentrations (Figure 4-1). The results of this test are independent from the selected EOS module, because flow and transport processes are not involved in these computations.

4.2 Verification Test 2: Calculation of the Mean Activity Coefficients of *NaCl* Solutions up to 6 m at 0°C, 25°C, 50°C, 80°C, 100°C, and 110°C

This test involves calculating the mean activity coefficients of *NaCl*, and the osmotic coefficient of *NaCl* solutions up to 6 molal of *NaCl* salt, at 0°C, 25°C, 50°C, 80°C, 100°C, and 110°C. The results are compared with data measured by Clarke and Glew (1985). This test case also verifies the calculated temperature dependency of activity coefficients. Note that comparisons of mean activity coefficients, rather than mean activities, are appropriate here, because no significant amounts of *Na* or *Cl* secondary species are calculated to form. Also, the results of this test are independent of the selected EOS module because flow and transport processes are not considered.

The mean activity coefficient of *NaCl* is calculated with:

$$ln(\gamma_{NaCl}) = \frac{ln(\gamma_{Cl}) + ln(\gamma_{Na})}{2} \tag{4.3}$$

The root-mean-square errors (RMSE) were also calculated and are smaller than 1%.

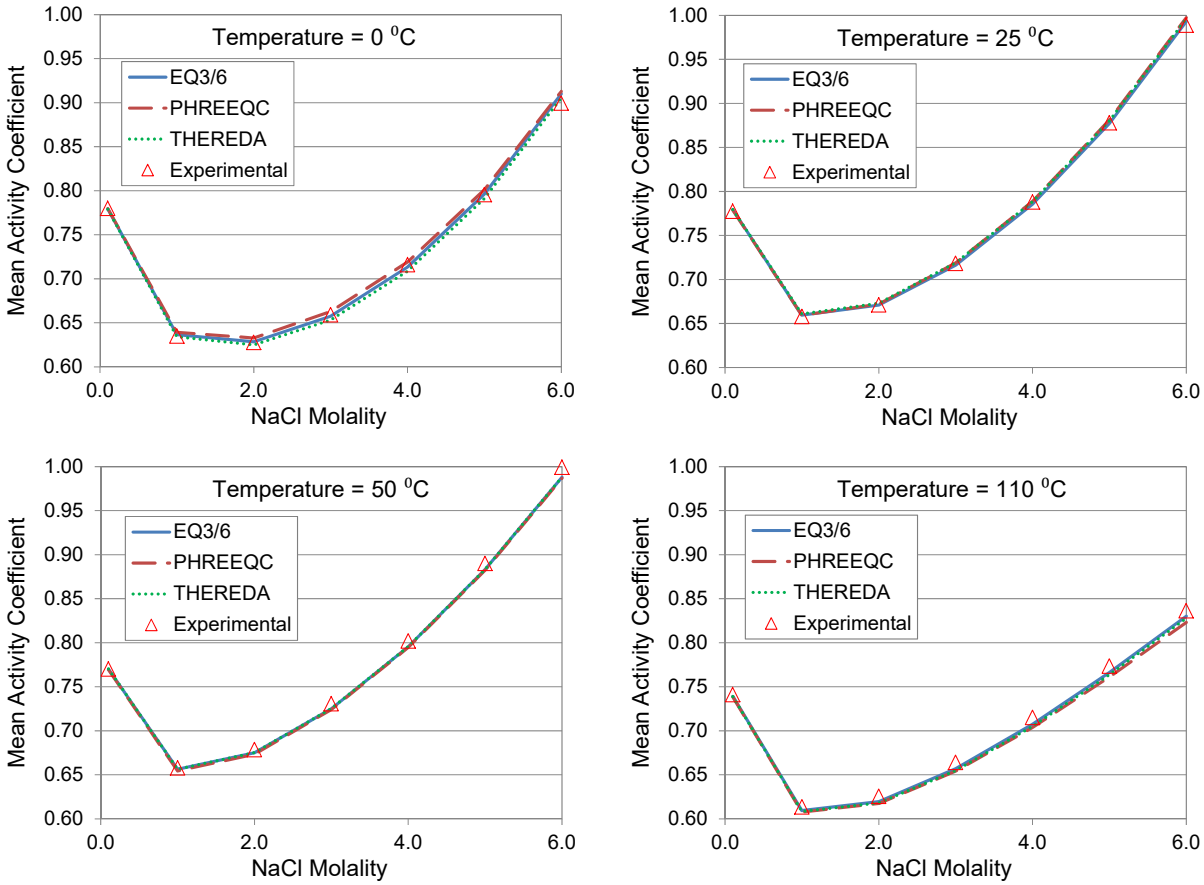

Figure 4-2. Examples of TOUGHREACT-calculated (lines) and measured (symbols) mean activity coefficients for NaCl solutions from 0°C to 110°C, using different thermodynamic databases. Measured data are from Clarke and Glew (1985).

4.3 Verification Test 3: Calculation of Water Vapor Pressure Lowering over $CaCl_2$ Solutions at Concentrations up to 9 m at 25°C

This test involves the calculation of the water vapor pressure over $CaCl_2$ solutions at concentrations up to 9 m $CaCl_2$ at 25°C and 1 bar, using TOUGHREACT with EOS3, and with vapor pressure lowering enabled (MOPR(24)=1). This test verifies the EOS3 capability to take into account vapor-pressure lowering caused by dissolved salts.

To verify the vapor-pressure-lowering effect, the vapor pressure of $CaCl_2$ solutions up to 9 m $CaCl_2$ was hand-calculated by taking the vapor pressure of pure water from the NIST steam tables (Wagner and Pruβ, 2002), then calculating the vapor pressure using a) Equation (2.3) and the water activity calculated by the Pizer ion-interaction model, and b) obtained from the air mass fraction, X_{air} (from output file *flow.out*) and the following equation:

$$P_v = \frac{(1 - X_{air}) p_{tot}}{1 - (1 - \frac{W_w}{W_{air}}) X_{air}} \tag{4.4}$$

where P_v is the vapor pressure, p_{tot} is total pressure, X_{air} is mass fraction of air, and W_w (18.061 g/mol) and W_{air} (28.96 g/mol) are the molecular weights of water and air, respectively. Equation (4.4) is derived according to the mass conservation law implemented in EOS3 (where the gas phase consists of air and water vapor only, Pruess et al., 1999). Results are shown in Figure 4-3. The relative differences are smaller than 1%.

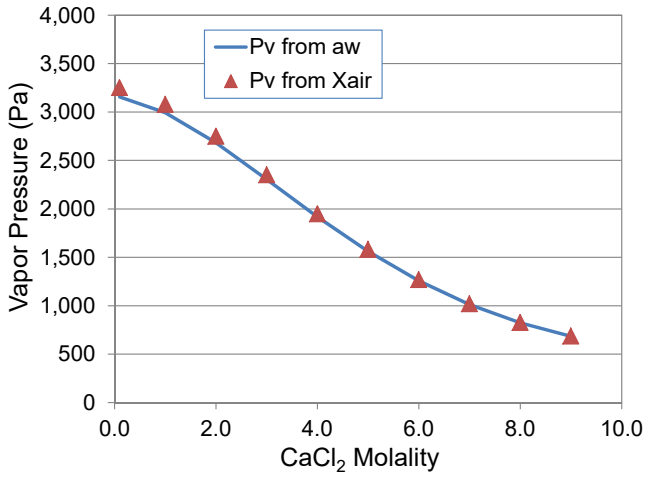

Figure 4-3. Comparison between the water vapor pressure derived from the water activity (a_w) and air mass fraction (X_{air}) computed with TOUGHREACT-EOS3 at increasing concentrations of dissolved $CaCl_2$ at 25°C and 1 bar (using converted EQ3/6 Pitzer thermodynamic database data0.ypf).

4.4 Verification Test 4: Calculation of Water Vapor Pressure Lowering over *$CaCl_2$* Solutions at Concentrations up to 9 m at 150°C, Including Capillary Suction

This test is similar to Test 3, using EOS4 instead of EOS3 to enable the effect of capillary suction, and with vapor pressure lowering enabled (MOPR(24)=1). This test verifies the EOS4 capability to account for vapor-pressure lowering caused by both capillary pressure and dissolved salts. The vapor pressure over $CaCl_2$ solutions at concentrations up to 9 molal of $CaCl_2$ and at variable temperatures is calculated using TOUGHREACT EOS4 at 150°C and 10 bar. In this case, the relative humidity (*Rh*) over a saline solution in a porous medium is reduced by both salinity and capillary suction.

The effect of capillary suction on vapor pressure is calculated in EOS4 as described in Section 2.2.2, using the vapor-pressure-lowering factor (F_v) defined with Equation (2.5) and arbitrarily setting the capillary pressure to a very high value (-1000 bar). The vapor-pressure-lowering factor (essentially a Poynting correction) was independently calculated using Equation (2.5) and molar

volume values from the NIST/ASME Steam Tables. The relative humidity values output from TOUGHREACT was then compared with $a_w F_v$ (Equation 2.8), taking the values of a_w from output file *chdump.out*. The vapor pressure (P_v) was hand-calculated using Equation (2.7), taking the vapor pressure of pure water at different temperatures (P^0_v) from the NIST/ASME Steam Tables and a_w values from output file *chdump.out*. The vapor-pressure values obtained in this way were then compared to the values indirectly computed by TOUGHREACT, obtained by P_{tot} - P_{air}, with P_{tot} and P_{air} being the total gas-phase pressure and air pressure output in file *flow.out*. Results are shown in Figure 4-4. The relative differences are smaller than 1%.

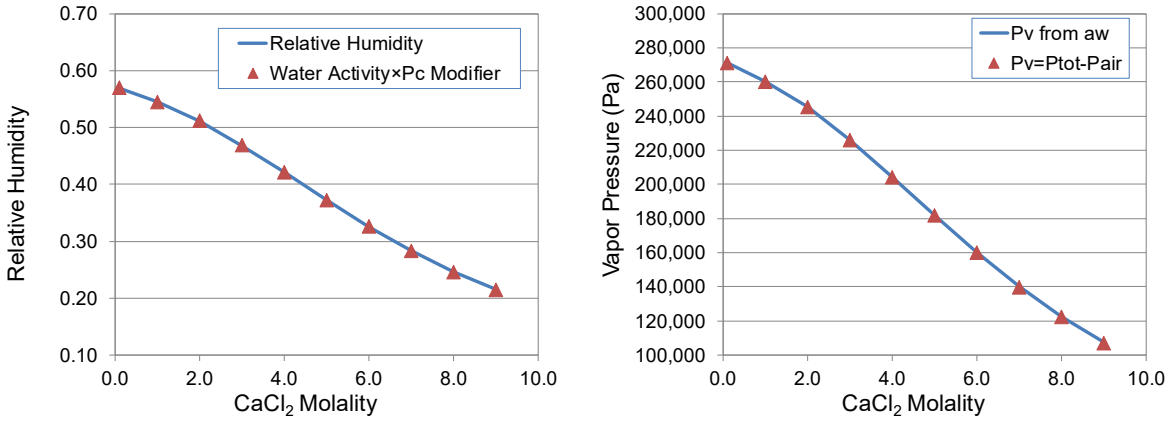

Figure 4-4. Comparison of water activity with relative humidity (left), and comparison of vapor pressures (right) at 150°C and 10 bar, as a function of $CaCl_2$ concentration (using converted EQ3/6 Pitzer thermodynamic database data0.ypf).

5 SAMPLE PROBLEMS

Sample problems included in the distribution package are described below.

5.1 Sample Problem 1: Evaporation of Black Sea Water

This sample problem consists of evaporating water from the Black Sea by incrementally removing H_2O from the solution, assuming thermodynamic equilibrium in the modeled system. The evaporation is carried out at a constant atmospheric CO_2 partial pressure ($\log(f_{CO2}) = -3.5$), using a water composition from Carpenter (1978), and assuming thermodynamic equilibrium. This problem is the same as Example 17b discussed in the PHREEQC v3.06 manual (Parkhurst and Appelo, 2013), except that it is run at a higher temperature (80°C) to verify the thermodynamic data functions of temperature.

This sample problem is run using EOS1 with only one single grid block ("batch" simulation) with a given volume of 1 m^3 and unit porosity. The GENER block in the *flow.inp* file is used to remove Component 2 (water) from the grid block at a negative rate of 1 kg/s. An arbitrary and constant time step length is specified (in the present case 0.1 s) and the total simulation time is specified such that enough water is removed to reach a desired maximum concentration factor (in

our case at least 100) but no so much as to remove more water than is available in the grid block (~ 1000 kg), a point at which the simulation would no longer converge. To avoid depressurization in the modeled grid block upon water withdrawal, its pore compressibility is set to a large value (10^{-2} Pa^{-1}) in the ROCKS block of the *flow.inp* file.

Results are shown in Figure 5-1 (left plots) as a function of the water concentration factor, calculated as the ratio of the concentration of a conservative species (in this case Br^-) to its initial concentration. The TOUGHREACT results from the *time.dat* output file (Figure 5-1, left plots) are compared with results of PHREEQC v3.06 for the same simulation setup (Figure 5-1, right plots). The simulations are performed using the PHREEQC v3.06 *Pitzer.dat* thermodynamic database (Plummer et al., 1988) and its conversion suitable for input to TOUGHREACT (*tk-pitz-phq3.06.dat*; Section 1.2). The results of the two codes for this problem match closely (Figure 5-1), showing precipitation of first calcite, then anhydrite, then halite as the water is progressively evaporated, accompanied by a decrease in water activity down to about 0.65.

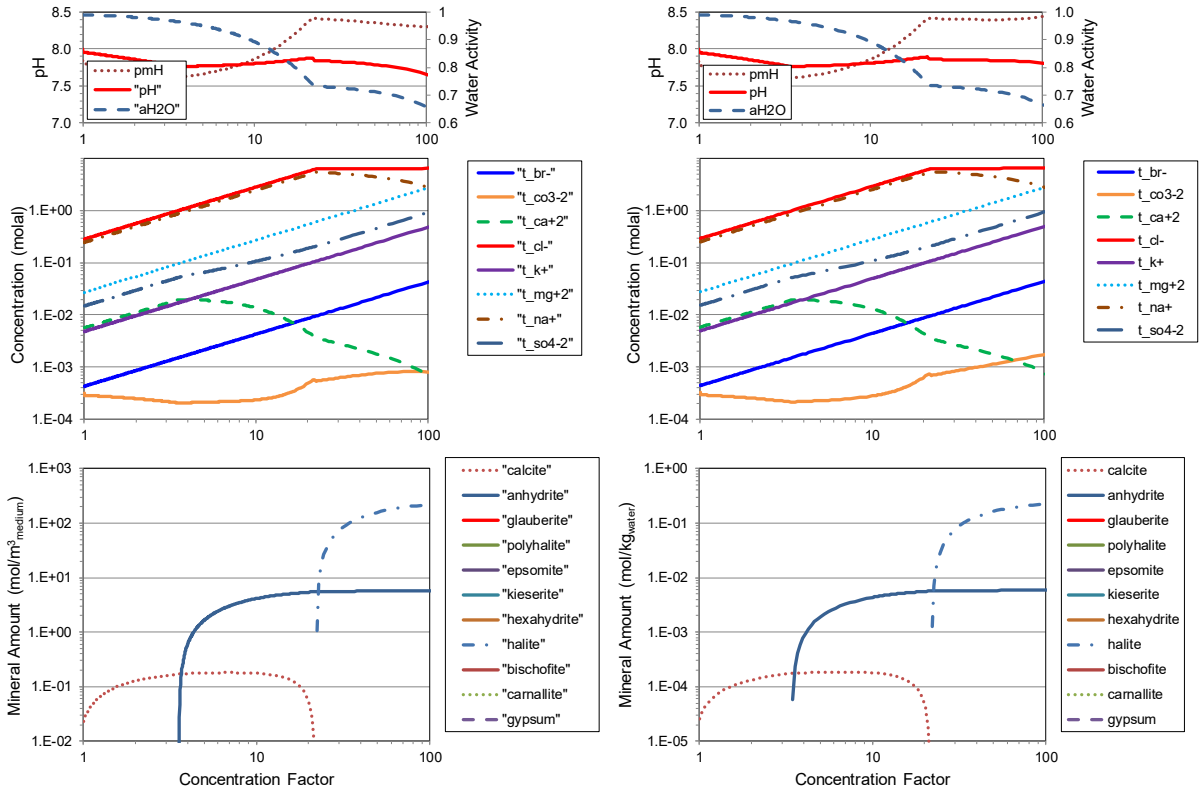

Figure 5-1. Evaporation of water from the Black Sea simulated with TOUGHREACT (left plots) and PHREEQC (right plots) at 80°C and 1 bar (pmH stands for –log[H^+ molality]).

5.2 Sample Problem 2: Evaporation of Produced Water

This sample problem is similar to Sample Problem 1 and is also run with EOS1. In this case, the evaporation of a produced water from the Williston Basin, North Dakota is simulated (USGS Produced Water Database well name Atlas 6092-13, 2012-10-16, Bakken Formation). The evaporation of the brine (TDS ~ 51,700 mg/L) is simulated with both TOUGHREACT and EQ3/6 (Wolery and Jarek, 2003), using the EQ3/6 *data0.ypf* Pitzer thermodynamic database (Wolery et al., 2004) and its conversion suitable for input to TOUGHREACT (*tk-pitz1.ypf.R2.dat*; Section 1.2). The simulation setup for this problem is identical to that of Sample Problem 1, using a single model grid block (1 m^3 volume and unit porosity) from which water is removed in finite increments. The brine concentration factor is calculated as the ratio of the concentration of a conservative species (in this case Br^-) to its initial concentration. A closed system and conditions of thermodynamic equilibrium are assumed, except for gypsum which is specified to react under fast (unlimiting) kinetic constraints to numerically smooth the transition from gypsum to anhydrite precipitation upon evaporation.

Results from the *time.dat* output file are shown on Figure 5-2 (left plots) and compare very well with results obtained with EQ3/6 (Figure 5-2, right plots). These figures show the brine evolving upon evaporation towards a very acidic $CaCl_2$ solution, accompanied by the precipitation of primarily anhydrite/gypsum, halite, sylvite and carnalite.

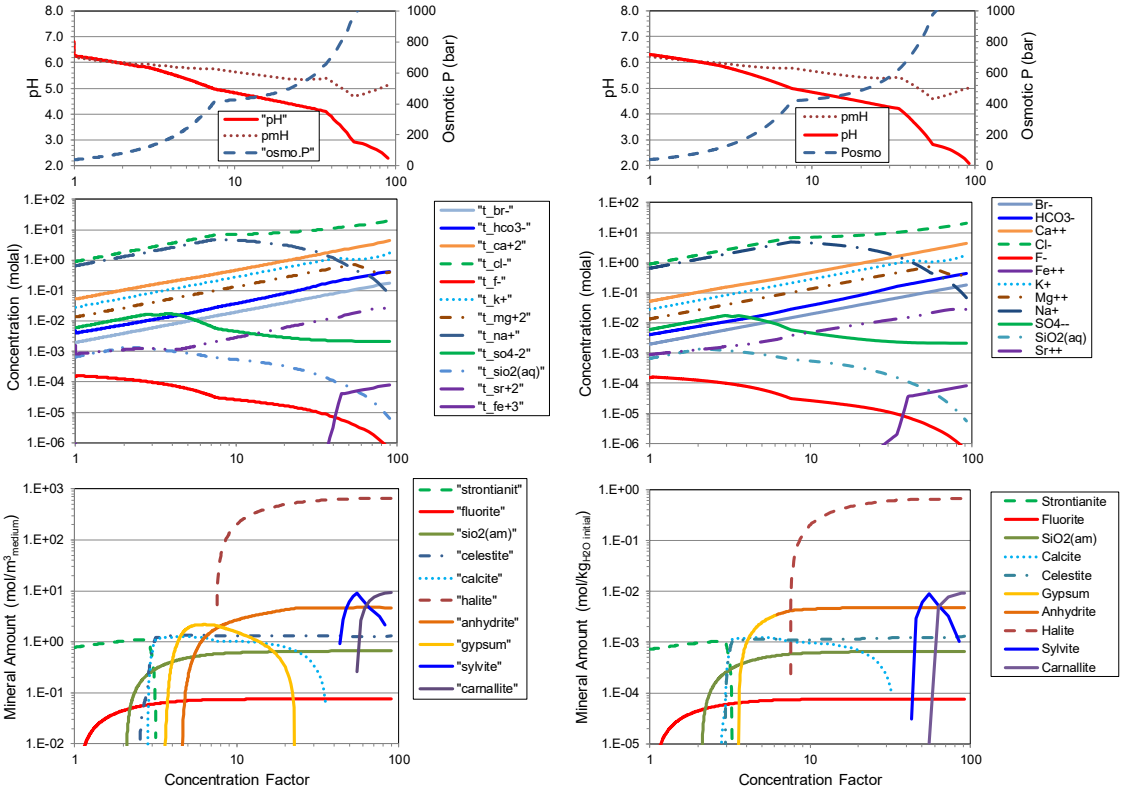

Figure 5-2. Evaporation of produced water from the Williston Basin simulated with TOUGHREACT (left plots) and EQ3/6 (right plots) at 25°C and 1 bar (pmH stands for –log[H^+ molality]). Note that the y-axis scales for the mineral amounts have different units that differ by a factor of about 1000.

5.3 Sample Problem 3: High-Temperature Aquifer Thermal Energy Storage

This sample problem relates to the geologic storage of thermal energy, using the Cranfield oil field (Natchez, Mississippi, USA) as a potential site for such operations because it has been extensively characterized for a deep CO_2 injection/storage pilot project (e.g., Hovorka et al., 2013). The concept for this problem is to heat the deep saline brine (from the Lower Tuscalosa Sandstone formation; total dissolved solids ~ 155,000 mg/L; Soong et al., 2016) then reinject it into that formation for energy storage. The problem is divided into two parts. In a first step, the brine is heated to assess the types and amounts of minerals that could precipitate upon heating and potentially create scaling problems; the pumping of the brine is not itself simulated (i.e., it is assumed that the brine has been pumped from the formation). In a second step, the heated brine fractionated from the minerals that precipitated upon heating is injected into the formation from which it originated from. These two steps involve two separate simulations as described below.

5.3.1 Brine Heating

This simulation is run using the EOS1 module (water only). It is set up as a "batch", one-grid block heating simulation (no flow), whereby the temperature of the brine, after some composition adjustments to represent in-situ conditions (Section 5.3.2), is increased by adding heat into the grid block in finite increments. The simulated time period is 10^5 seconds (~28 hours), adding heat at a rate of 4420 J/s, assuming a closed system with minerals set to precipitate under kinetic constraints. The heating rate was determined (from steam tables and the total simulation time) to raise the brine temperature from its natural in-situ value of 126°C to about 240°C. To avoid a pressure build-up in the single model grid block, the pore compressibility is set to a large value in file *flow.inp* (10^{-2} Pa^{-1}). Results from the *time.dat* output file are then plotted (after conversion to mass units for minerals) to examine the evolution of the water chemistry and amounts of solids precipitated upon heating. Heating the brine results in the precipitation of mostly anhydrite with some calcite and Mg silicate minerals (modeled as talc), and in a steady but slight pH decrease from about 5.5 to 5.2 (Figure 5-3).

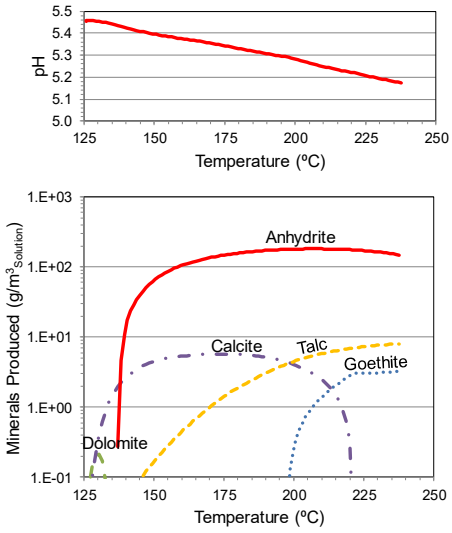

Figure 5-3. Simulated evolution of pH and minerals precipitated upon heating (closed system) a brine from the Lower Tuscalosa Sandstone formation, Cranfield oil field, Mississippi.

5.3.2 Brine Injection

This simulation is run using the EOS7 module, which considers the modeled brine as a mixture of component "water" and component "reference brine". The default NaCl mass fraction of the reference brine in EOS7 is 0.25, therefore the mass fraction of the reference brine (X_b) in the modeled system is set to a value (0.62) that is consistent with the salinity of the system being modeled (i.e., total salinity X_{NaCl}=0.62×0.25=0.155 wt. fraction).

The numerical mesh for this simulation (courtesy C. Doughty, LBNL) is set up as radial 2-dimentional (x-z) grid, with a single injection/pumping well. The model set-up and hydrogeologic inputs are the same as those presented by Doughty and Freifeld (2013) for simulations of CO_2 injection at the Cranfield site, and includes vertically heterogenous but horizontally homogenous geologic layers (Figure 5-4). The model domain is discretized with Δx increasing logarithmically away from the well, starting with the size of the well/borehole diameter (0.2 m, at the left model boundary). A constant hydrostatic pressure boundary is located 4 km away from the well (right model boundary). Vertically the model domain is discretized into 20 regular increments Δz of 1.2 m. The top and bottom model boundaries are close to flow but open to heat transport using the semi-analytical heat exchange option implemented in TOUGH2.

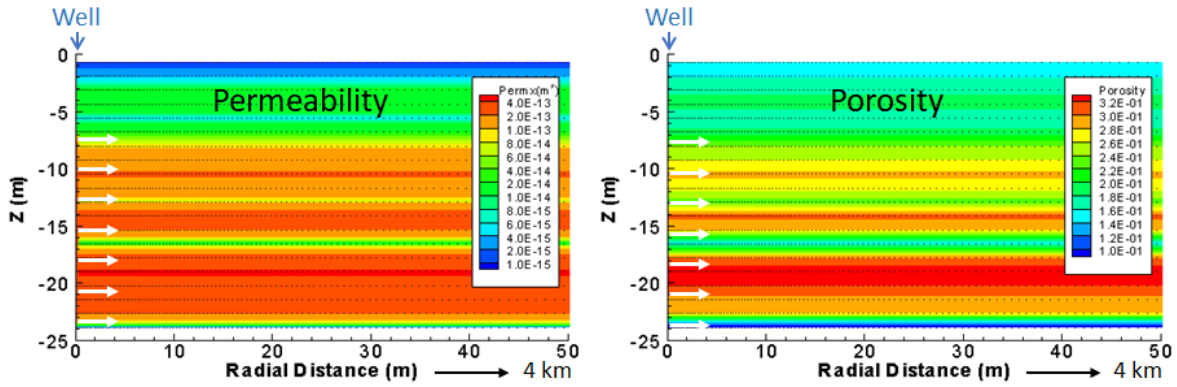

Figure 5-4. Permeability (m^2) and porosity fields for the reactive transport simulation of brine injection. The white arrows cover the vertical extent of the well perforated interval. Black dots show the model grid blocks centers.

To minimize computing time, this sample problem is set up to simulate only a three-month injection period. However, the GENER file provided for this problem includes 5 cycles of 3-month injection + 3-month rest + 3-month withdrawal + 3-month rest for a total period of five years (courtesy C. Doughty, LBNL). The injection (and withdrawal) rate is assumed to be 3 kg/s (~43 gpm); it is applied directly at the top of the perforated interval (at z =-7.9 m), and the latter is given a high vertical permeability (0.233×10^{-9} m^2; ROCKS material name INJCT).

The brine composition is taken from Soong et al. (2019) for the Lower Tuscalosa sandstone, and the mineralogy of that formation is taken as the average mineral amounts reported by Lu et al. (2012). In a first step (not part of this sample problem), to obtain chemically near-steady initial

conditions, the brine-mineral system was reacted for a period of 1000 years at the formation temperature (126°C) and pressure (300 bar). The mineral reactive surface areas were initially estimated from spherical grain sizes of 100 microns then modified, together with the mineral assemblage, as necessary to obtain a reasonable agreement between the reported brine chemistry and mineralogical data at the end of the 1000-year simulation (Figure 5-5).

The brine resulting from these initial manipulations is used as the initial formation water for the injection simulation. The composition of the injected water is taken as the composition of the formation brine heated to 180°C, as determined from the heating simulation described in Section 5.3.1, after fractionation of the solids predicted to precipitate at that temperature (mostly anhydrite, see Figure 5-3).

Analyte	Brine Composition* (ppm)	1000-year Reacted (ppm)	Reported Range** (mg/L)
pH	~6 @ 25°C	5.46 @ 126°C	5.6 - 6.4 @ 25°C
TDS (calc)	150714	151109	
density (kg/L)	1.115 (calc)		
Cl-	92223	92206	86212-95300
SO4-2	238	238	25-55
HCO3-	NA	103	278-580
HS-	NA	1	NA
Br-	432	432	297-437
SiO2(aq)	NA	59	NA
Al+3	1.06	1.7E-07	0.25-9
Ca+2	11798	12943	7636-11700
Mg+2	1035	468	770-1052
Fe+2	124	31	95-532
K+	412	491	272-604
Na+	43743	43432	39581-49192
Sr++	696	696	512-723
B+3	1.9	2	NA
Ba+2	9.6	9.5	43-99

* Soong et al. (2016)
**Lu et al. (2012)

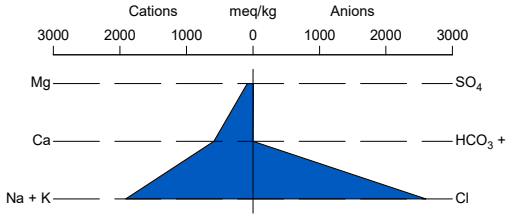

Minerals	Reacted Sat. Index	Composition (wt.%)
quartz	0.00	79.40
Fe-chlorite	0.00	11.80
kaolinite	-0.04	3.10
illite	0.02	1.30
calcite	0.00	1.10
K-feldspar	-0.41	0.50
albite	0.00	0.50
dolomite	0.00	0.40
ankerite	0.00	0.10
FeS (as pyrrhotite)	0.00	0.10
anhydrite	-0.08	
chalcedony	-0.21	
barite	-0.25	
goethite	-0.53	
strontianite	-0.57	
siderite	-1.15	

Figure 5-5. Brine chemistry, formation mineralogy, and potential secondary minerals selected for the reactive transport simulation of brine injection.

The results of the simulation at three months of continuous injection are shown on Figure 5-6 to Figure 5-8. The permeability increases near the well as the result of mostly quartz dissolution (Figure 5-6). Heating and the mobilization of silica results in the precipitation of Mg silicates near the well (modeled as talc and chlorite), however in amounts that are insufficient to offset the effect of quartz dissolution (Figure 5-7).

Further away from the well, some replacement of dolomite by calcite is predicted in the zone with highest temperatures; reversely, minor replacement of calcite by dolomite takes place at lower temperature (Figure 5-8). These reactions do not alter permeability significantly. A plume of lower pH (down to ~ 4.8) develops mostly following the shape of the elevated temperature plume (Figure 5-8).

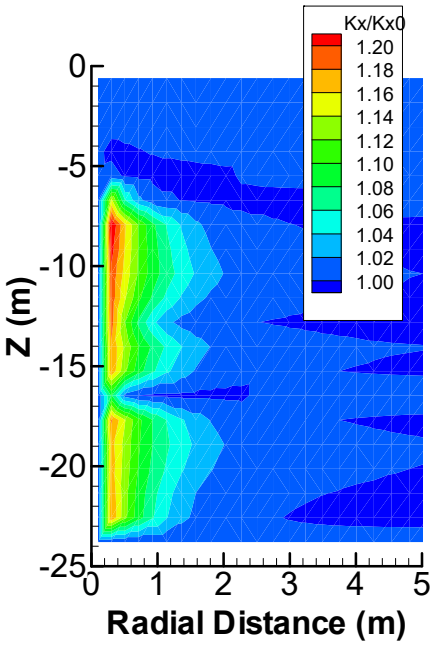

Figure 5-6. Computed permeability increase after 3 months of brine injection, contoured as the ratio of current (3 months) to initial permeability.

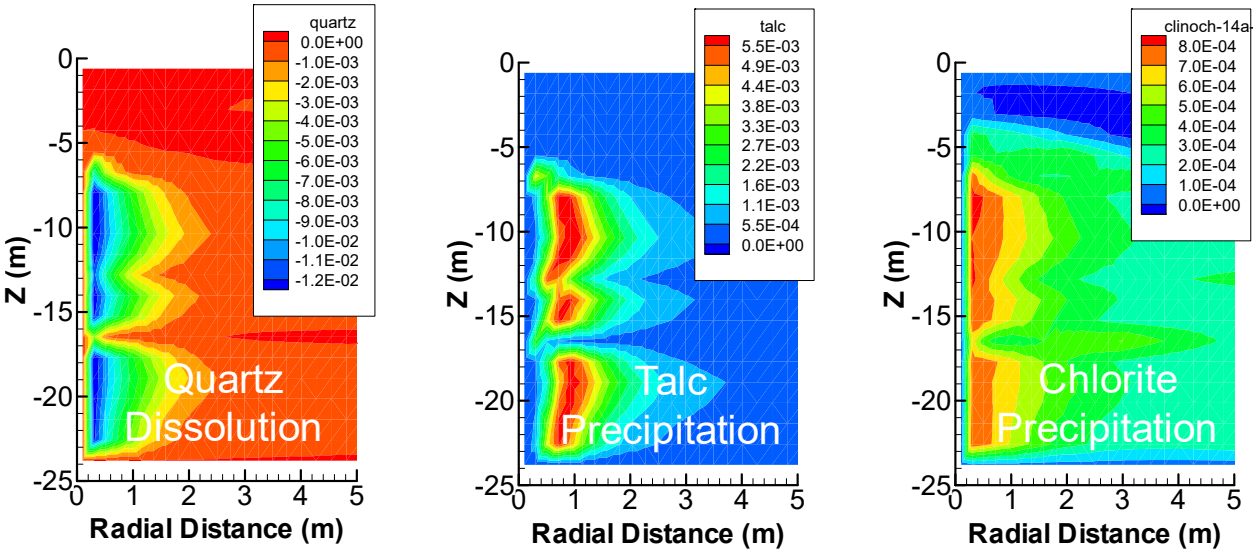

Figure 5-7. Computed total volume fraction change of main minerals dissolving (negative) and precipitating (positive) near the modeled injection well after 3 months of brine injection.

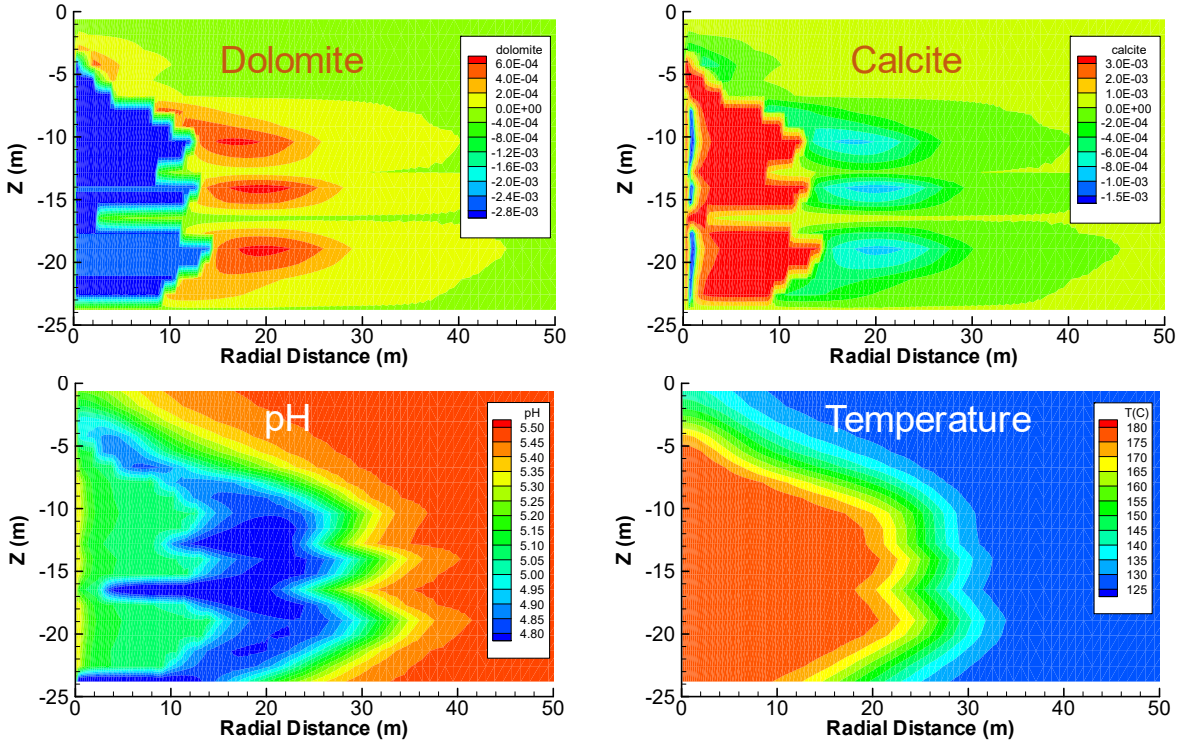

Figure 5-8. Computed total volume fraction change of main reacting minerals away from the well (top) together with the pH and temperature plumes (bottom) simulated after 3 months of brine injection.

5.4 Sample Problem 4: Simulation of Reverse Osmosis Through a Desalination Membrane

This sample problem is provided to help users setup a reverse osmosis (RO) membrane desalination simulation. The development of this capability is new, experimental and still evolving, and therefore this sample problem will be most useful to users involved in further developing this capability, such as implementing more sophisticated models of mixing/dispersion and membrane "clogging", which at present are implemented in a fairly crude manner (see Section 3.2).

This problem consists of simulating the reverse osmosis of a saline solution (32,000 ppm NaCl) at 55 bar total pressure and a temperature of 25°C. The modeled membrane properties and flow/operating conditions are consistent with data reported by DOW (2018) for their spiral-wound RO element Filmtech SW30HR-380. The simulation of osmosis is enabled by setting MOPR(25) =1 in input file *flow.inp* (see Section 3.1).

A typical spiral-wound RO module is shown on the upper part of Figure 5-9. RO through one feed/membrane/permeate assembly in such module is simulated in two dimensions as shown on the lower part of Figure 5-9, using the new code capabilities described in Sections 2.3 and 2.4.

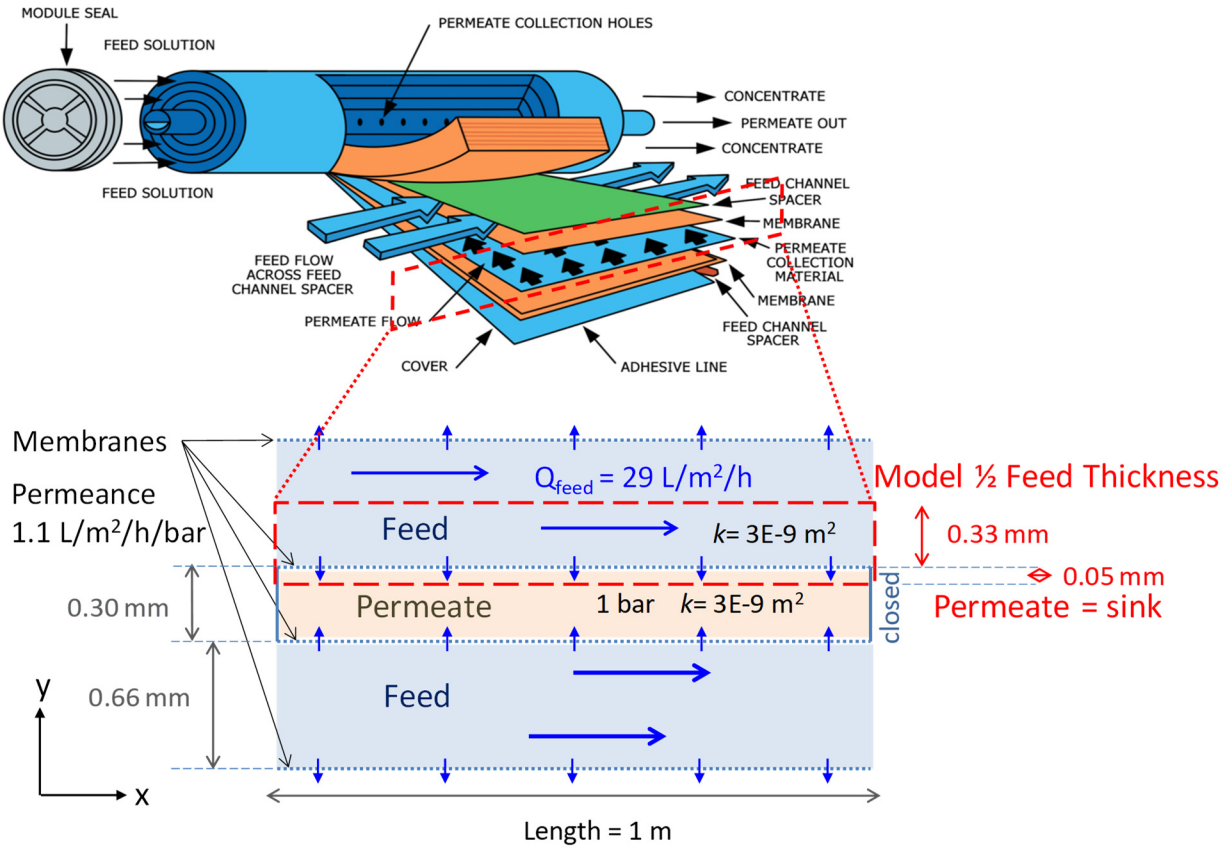

Figure 5-9. Simulation of reverse osmosis in a 1-meter long spiral-wound RO module. The top figure illustrates a typical industrial spiral-wound RO module. The bottom figure shows an enlarged section cutting through one permeate channel sandwiched between two feed channels, and their respective modeled thicknesses. The modeled domain is shown by the dashed red line, together with some of the model input parameters.

The modeled system is simplified in two dimensions and takes advantage of symmetry by considering only half the feed channel thickness and one membrane (Figure 5-9). This allows treating the top of the model (mid-point in the feed channel) as a no-flow boundary. The length of the model domain is set to 1 m, corresponding to the length of a typical spiral-wound RO module; it is discretized into 200 Δx increments of 5 mm. The (finite volume) model grid blocks are given an arbitrary depth also set to 1 m (3rd dimension in a direction perpendicular to Figure 5-9, not explicitly modeled). For convenience, the grid blocks representing the feed channel directly above the membrane (adjacent to the permeate) are set with y coordinate = 0, thus the feed channel grid blocks have positive y coordinates whereas the permeate grid blocks have negative y coordinates (see the MESH input file).

The modeled half feed channel is discretized in the y direction into 11 continuous layers increasing in thickness (Δy) from 10 to 50 microns away from the membrane. A specified flux is applied at the inlet of the feed channel on the left side of the model. A downstream pressure of 55 bar is maintained at the feed outlet on the right side of the modeled domain. The feed channel

permeability is set to a value (3×10^{-9} m^2) that yields a pressure drop of about 0.5 bar from one end of the RO module to the other (over the 1-meter flow path) and that does not limit the applied feed flux. The porosity of the feed channel is given an arbitrary high value of 0.98.

The influx of feed water is calculated from the spiral-wound module manufacturer's reported total permeate flux (24.6 m^3/day for a total membrane surface of 35 m^2) and recovery of permeate (8% of the feed), together with the modeled feed channel area perpendicular to the feed flow direction ($0.66\times10^{-3}\times1$ m^2). Using these values, the specified feed mass influx rate in half the channel thickness is calculated to be about 0.051 kg/s, which corresponds to a high feed velocity of about 0.15 m/s. In the GENER input file, the flux is weight-averaged by the thickness of each layer and distributed in proportionate amounts into the first grid block of each feed model layer. This weight averaging is required for the POISEUILLE option (see further below) to function properly.

The permeate channel is discretized into 4 continuous model layers increasing in thickness from 10 to 17 microns away from the membrane. A constant 1-bar pressure is applied in the outer-most layer of the permeate (i.e., at the model bottom boundary) while other boundaries in the permeate channel are closed to flow. As such, the permeate channel is modeled as a sink for all feed water penetrating through the membrane.

The RO membrane is treated as a special connection that is closed to advective transport but open to diffusive transport using Equation (2.15) for water. This connection is automatically enabled between grid blocks with material names *perm1* and *feed1* in the ROCKS block of input file *flow.inp* (it is also enabled for connections set with ISOT=10, see Section 3.1). This option is enabled when the membrane permeance for use with Equation (2.15) is entered in file *solute.inp* (Section 3.2). In the present case, the permeance is set to 1.1 L $m^{-2}h^{-1}bar^{-1}$, which corresponds to the value reported by Wagner et al. (2009, their Table 1) for the DOW membrane SW30HR. Entering the membrane permeance avoids having to discretize the membrane itself (which has a typical thickness of 200 nm), which would require simulations with a very fine spatial discretization and thus very small time steps (although the membrane could be discretized if desired and with commensurate computing power, and given material name *ROmem*).

When MOPR(25) in file *flow.inp* is set to a value > 0 to enable osmosis, the diffusion coefficients in the membrane (i.e., for transport between grid blocks with material names *perm1* and *feed1*) are automatically read from the thermodynamic database (see Section 3.1). In the present case, the diffusion of aqueous species through the membrane is restricted by setting their diffusion coefficient to a very low value (10^{-30} m^2/s). Salt rejection is not currently rigorously implemented but salt leakage could be approximated by increasing these diffusion coefficients. In contrast, the diffusion coefficients used within the feed and permeate flow channels are automatically set to the value specified in the *solute.inp* file (same for all aqueous species). The water diffusion coefficient within the membrane is entered as 2×10^{-10} m^2/s in the thermodynamic database (from Geise et al. 2016, their Figure 16), whereas the water self-diffusion coefficient outside the membrane is set internally in the code at 2.3×10^{-9} m^2/s at 25°C (from Mills, 1973).

Within the feed channel, the Poiseuille flow option (Section 2.4) is enabled by entering a POISEUILLE input block in the *flow.inp* file (Section 3.1) defining the coordinates of the surface (line in 2D) along which the velocity drops to zero (i.e., at the membrane surface). In our case this surface extends from <x;y> = <0; -200 nm> to <x;y> = <1 m; -200 nm>, and the the total thickness of the feed channel (not half!) is specified as 0.66×10^{-3} m. In addition, in the MESH input file, a new parameter *ipois* = 1 is entered on each record of the feed channel grid blocks (after the grid block coordinates), to indicate that the scaling of velocities will be applied to these grid blocks (see Section 3.1).

The simulation is run for 60 seconds in time steps of ~ 0.03 seconds dictated by the high flow velocity and a unit Courant number (the latter is entered in file *solute.inp*). The computed distribution of osmotic pressure in the feed channel after this time (at essentially steady state) is shown in Figure 5-10, for a case considering no mixing/dispersion.

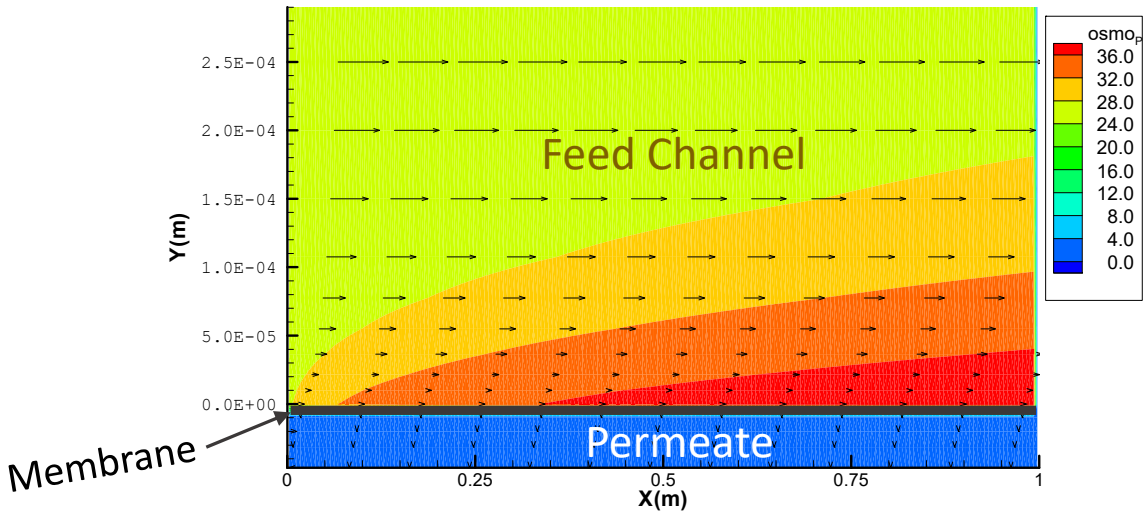

Figure 5-10. Simulated distribution of osmotic pressure (in bar) along the modeled spiral-wound RO module shown in Figure 5-9, without mixing/dispersion. Arrows indicate the flow direction and relative magnitude.

When using the osmosis option by setting MOPR(25) > 0, two additional output files are generated. Output file *osmo-flux.dat* shows, for each and every grid block, the cumulative water amount gained or lost, the water flux, the water activity (aw(n)), and the term *a'* in Equation (2.12) (aterm(n)), at time intervals specified in file *flow.inp*. This file is typically used for debugging purpose only. The second output file, *permeate.out*, shows the total permeate flux (in kg/s and L/day) for the system modeled (in the present case, for a membrane surface of 1 m^2), at time step intervals specified file *solute.inp*. This file was used to generate Figure 5-11, which compares the effect of dispersion/mixing on the amount of permeate generated for the full spiral-wound module membrane surface of 35 m^2. The permeate flux computed with dispersion is close to the manufacturer's reported value of 24.6 m^3/day (Figure 5-11). The significantly lower value computed without dispersion reflects the strong "concentration polarization" shown on Figure 5-10 when no mixing takes place. The dispersion coefficient is entered in file *solute.inp* (see Section

3.2); in the present case a value of ~0.01 m provides the best results and near maximum flux (i.e., the flux does not increase significantly with higher dispersion values).

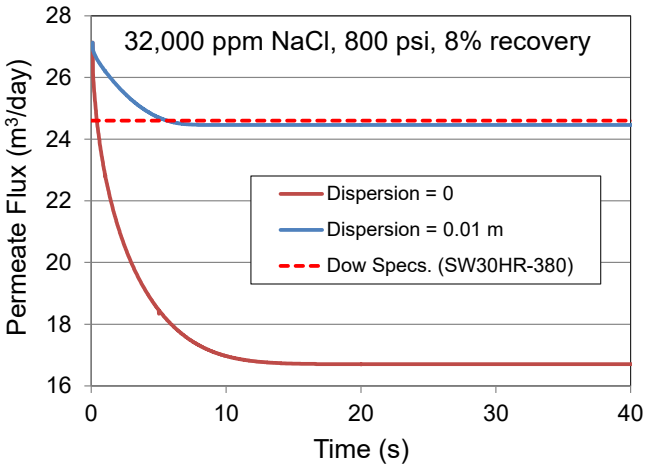

Figure 5-11. Computed permeate flux as a function of time for cases with and without mixing/dispersion, scaled up for a total spiral-wound module membrane surface of 35 m^2, compared with the membrane manufacturer's specification (dashed line).

6 REFERENCES

Alai, M., M. Sutton, and S. Carroll, 2005, Evaporative evolution of a Na–Cl–NO3–K–Ca–SO4–Mg–Si brine at 95 °C: Experiments and modeling relevant to Yucca Mountain, Nevada, *Geochemical Transactions*, 6 (2) 31-45.

Carpenter, A.B., 1978, Origin and chemical evolution of brines in sedimentary basins: Oklahoma Geological Survey Circular 79, p. 60–77.

Clarke, E. C. W, and D. N. Glew, 1985, Evaluation of the thermodynamic functions for aqueous sodium chloride from equilibrium and calorimetric measurements below 154 °C, *Journal of Physical and Chemical Reference Data*, 14, 489-610Doughty, C. and B. M. Freifeld, Modeling CO_2 injection at Cranfield, Mississippi: Investigation of methane and temperature effects, *Greenhouse Gas Science and Technology*, 3, 475-490, 2013.

DOW, 2018, FILMTEC™ SW30HR–380 Element, high rejection, seawater reverse osmosis membranes. Product Data Sheet, The Dow Chemical Company Form No. 609-00390, Rev. 1, June 2018.

Felmy, A. R., H. Cho, J. R. Rustad, and M. J. Mason, 2001, An aqueous thermodynamic model for polymerized silica species to high ionic strength, *J. Solution Chem.*, 30(6), 509–525.

Geise, G. M., Paul, D.R., and B. D. Freeman, 2016, Fundamental water and salt transport properties of polymeric materials, *Progress in Polymer Science*, 39, 1– 42

Harvie, C.E. and Weare, J.H., 1980, The Prediction of Mineral Solubilities in Natural Waters: The Na–K–Mg–Ca–Cl–SO_4–H_2O System from Zero to High Concentration at 25°C, *Geochimica et Cosmochimica Acta*, 44, (7), 981-997.

Harvie, C. E., Moller, N., and J. H. Weare, 1984, The Prediction of Mineral Solubilities in Natural Waters: The Na-K-Mg-Ca-H-Cl-SO_4-OH-HCO_3-CO_3-H_2O System to High Ionic Strengths at 25°C, *Geochimica et Cosmochimica Acta*, 48, (4), 723-751.

Hovorka, S. D., Meckel, T. A., and R. H.Treviño, 2013, Monitoring a large-volume injection at Cranfield, Mississippi—Project design and recommendations, *International Journal of Greenhouse Gas Control*, 18, 345-360.

Lu, J., Kharaka, Y., Thordsen, J., et al., 2012, CO_2–rock–brine interactions in Lower Tuscaloosa Formation at Cranfield CO2 sequestration site, Mississippi, U.S.A. *Chemical Geology* 291 (2012) 269–277.

Mills, R., 1973, Self-diffusion in normal and heavy water in the range 1-45°, *Journal of Physical Chemistry*, (7), 5, 685-688.

Monnin, C., 1994, Density calculation and concentration scale conversions for natural waters, *Comput. Geosci.*, 20 (10), 1435-1445.

Parkhurst, D. L., and C. A. J. Appelo, 2013, Description of Input and Examples for PHREEQC Version 3—A Computer Program for Speciation, Batch-Reaction, One-Dimensional Transport, and Inverse Geochemical Calculations. Chapter 43 of Section A, Groundwater Book 6, Modeling Techniques, U.S. Department of the Interior U.S. Geological Survey, Techniques and Methods 6–A43, 497 pp.

Pitzer, K. S. 1973, Thermodynamics of electrolytes, I. Theoretical basis and general equations, *J. Phys. Chem.*, 77, 268– 277.

Pitzer, K. S., and G. Mayorga, 1973, Thermodynamics of electrolytes. II. Activity and osmotic coefficients for strong electrolytes with one or both ions univalent, *J. Phys. Chem.*, 77, 2300-2307.

Pitzer, K.S., 1991, Ion Interaction Approach: Theory and Data Correlation, Chapter 3 of Activity Coefficients in Electrolyte Solutions, 2nd Edition, Pitzer, K.S., ed. Boca Raton, Florida: CRC Press, TIC: 251799.

Plummer, L. N., Parkhurst, D. L., Fleming, G. W., and S. A. Dunkle, 1988, A computer program incorporating Pitzer's equations for calculation of geochemical reactions in brines, U.S. Geol. Surv. Water Resour. Invest. Rep., 88-4153, 310 pp.

Pruess, K., 1991, TOUGH2 – A General-Purpose Numerical Simulator for Multiphase Fluid and Heat Flow, Report LBL-29400. Berkeley, California: Lawrence Berkeley Laboratory. ACC: NNA.19940202.0088.

Pruess, K., C. Oldenburg, and G. Moridis, 1999, TOUGH2 User's Guide, Version 2.0, LBNL 43134, Lawrence Berkeley National Laboratory, Berkeley, California.

Rard J. A., and A. M. Wijesinghe, 2003, Conversion of parameters between different variants of Pitzer's ion-interaction model, both with and without ionic strength dependent higher-order terms, *J. Chem. Thermodynamics*, 35, 439-473.

Rogers, P. S. Z., 1981, Ph.D dissertation, Earth Sciences Division, University of California, Berkeley, CA, March, 1981.

Sonnenthal, E. L., Spycher, N., Xu, T., and L. Zheng, 2018, TOUGHREACT V3.6-OMP Reactive-Transport User Guide – A Parallel Simulation Program for Non-Isothermal Multiphase Geochemical Reactive Transport. Lawrence Berkeley National Laboratory, Report LBNL-DRAFT.

Sonnenthal, E. L., and N. Spycher, 2001, Drift-Scale coupled processes (DST and THC seepage) models. AMR N0120/U0110 Rev.01, Yucca Mountain Project, Lawrence Berkeley National Laboratory, Berkeley, California, MOL.20010314.0003.

Sonnenthal E., A. Ito, N. Spycher, M. Yui, J. Apps, Y. Sugita, M. Conrad, and S. Kawakami, 2005. Approaches to modeling coupled thermal, hydrological, and chemical processes In the Drift Scale Heater Test at Yucca Mountain. *International Journal of Rock Mechanics and Mining Sciences, 42, 698-719*.

Soong, Y., Howard, B. H., Dilmore, R. M., Haljasmaa, I., Crandall, D. M., Zhang, L., Zhang, W., Lin, R., Irdi, G.A., Romanov, V. N., and T. R. McLendon, 2016, CO_2/brine/rock interactions in Lower Tuscaloosa formation. *Greenhouse Gas Sci Technol*. **6**:824–837 (2016)

Spycher N. F., Sonnenthal, E. L., and J. A. Apps, 2003, Fluid flow and reactive transport around potential nuclear waste emplacement tunnels at Yucca Mountain, Nevada, *J. of Contam. Hydrol.*, 62-63, 653-673.

Wijmans, J.G. and R.W. Baker, 1995, The solution-diffusion model: a review, *J. Membrane Science* 107, 1-21.

Wagner, W. and A. Pruβ, 2002, The IAPW formulation 1995 for the thermodynamic properties of ordi-nary water substance for general scientific use, *Jour. Phys. Ref. Data, 31*, 387-535.

Wolery T. J., and S. A. Daveler, 1992, EQ6, A Computer program for Reaction Path Modeling of Aqueous Geochemical System: Theoretical Manual, User's Guide, and Related Documentation (version 7.0), Lawrence Livermore National Laboratory.

Wolery, T. J. and R. L. Jarek, 2003, EQ3/6, Version 8.0, Software User's Manual, Software Document Number 10813-UM-8.0-00, U.S. Department of Energy, Office of Civilian Radioactive Waste Management, Office of Repository Development, 1261 Town Center Drive, Las Vegas, Nevada 89144, 2003.

Wolery T., Jove-Colon C., Rard., J., and A. Wijesinghe., 2004, Pitzer Database Development: Description of the Pitzer Geochemical Thermodynamic Database data0.ypf. Appendix I in In-Drift Precipitates/Salts Model (P. Mariner) Report ANL-EBS-MD-000045 REV 02. Las Vegas, Nevada: Bechtel SAIC Company.

Xu, T., Sonnenthal E., Spycher N., and K. Prues, 2004, TOUGHREACT Users'Guide: A Simulation Program for Non-isothermal Multiphase Reactive Geochemical Transport in Variably Saturated Geologic Media. Lawrence Berkeley National Laboratory Report LBNL-55460.

Xu, T., and K. Pruess, 2001, Modeling multiphase non-isothermal fluid flow and reactive geochemical transport in variably saturated fractured rocks: 1. Methodology, *American Journal of Science*, 301, 16-33.

Xu, T., and K. Pruess, 1998, Coupled modeling of non-isothermal multiphase flow, solute transport and reactive chemistry in porous and fractured media: 1. Model development and validation, Lawrence Berkeley National Laboratory Report LBNL-42050, Berkeley, California, 38 pp.

Zhang,G. Z. Zheng, and J. Wang, 2005, Modeling reactive geochemical of concentrated aqueous solutions, Water Resour. Res., 41, W02018, doi: 10.1029/2004WR003097.

APPENDIX A. IMPLEMENTED PITZER ION-INTERACTION MODEL

A.1 FORMULATION OF THE PIZTER ION-INTERACTION MODEL

A generally accepted form of the Pitzer model was formulated in Harvie et al. (1984) and called the HMW formulation (model). This model has been implemented in TOUGREACT. In the HMW model, water activity is formulated as:

$$Ln(a_{H_2o}) = -\frac{m_w}{1000}(\sum_{i=1}^{N} m_i)\phi \tag{A1}$$

where a_{H_2o} is water activity, m_i is molality of species i, m_w is molecular weight of water, N is the number of species in the system, and ϕ is the osmotic coefficient, defined as:

$$\begin{aligned}
&\sum_{i=1}^{N} m_i(\phi - 1) = 2(-\frac{A^{\Phi} I^{\frac{3}{2}}}{1+1.2\sqrt{I}}) \\
&+ \sum_{c=1}^{N_c}\sum_{a=1}^{N_a} m_c m_a (B_{ca}^{\Phi} + ZC_{ca}) \\
&+ \sum_{c}\sum_{c'=c+1} m_c m_{c'} (\Phi_{cc'}^{\phi} + \sum_{a=1} m_a \psi_{cc'a}) \\
&+ \sum_{a}\sum_{a'=a+1} m_a m_{a'} (\Phi_{aa'}^{\phi} + \sum_{c=1} m_c \psi_{aa'c}) \\
&+ \sum_{n=1}^{N_n}\sum_{c=1}^{N_c} m_n m_c \lambda_{nc} + \sum_{n=1}^{N_n}\sum_{a=1}^{N_a} m_n m_a \lambda_{na} \\
&+ \sum_{n=1}^{N_n}\sum_{c=1}^{N_c}\sum_{a=1}^{N_a} m_n m_c m_a \zeta_{nca}
\end{aligned} \tag{A2}$$

where I is the ionic strength, defined as $I = \frac{1}{2}\sum_{k=1}^{N} z_k^2 m_k$, and z_k is the electrical charge of species k. The subscripts c, a, and n denote cations, anions, and neutral species, respectively. The activity coefficients of cations (γ_M), anions (γ_X), and neutral species (γ_N) are respectively calculated as:

$$\begin{aligned}
&\ln \gamma_M = Z_M^2 F + \sum_{a=1}^{N_a} m_a (2B_{Ma} + ZC_{Ma}) \\
&+ \sum_{c=1} m_c (2\Phi_{Mc} + \sum_{a=1} m_a \psi_{Mca}) \\
&+ \sum_{a}\sum_{a'=a+1} m_a m_{a'} \psi_{aa'M} \\
&+ |Z_M| \sum_{c=1}^{N_c}\sum_{a=1}^{N_a} m_c m_a C_{ca} \\
&+ 2\sum_{n=1}^{N_n} m_n \lambda_{nM}
\end{aligned} \tag{A3}$$

$$\ln \gamma_X = Z_X^2 F + \sum_{c=1}^{N_c} m_c (2B_{cX} + ZC_{cX}) + \sum_{a=1} m_a (2\Phi_{Xa} + \sum_{c=1} m_c \psi_{Xac}) + \sum_{c} \sum_{c'=c+1} m_c m_{c'} \psi_{cc'X} + |Z_x| \sum_{c=1}^{N_c} \sum_{a=1}^{N_a} m_c m_a C_{ca} + 2\sum_{n=1}^{N_n} m_n \lambda_{nX} \quad \text{(A4)}$$

$$\ln \gamma_N = \sum_{a=1}^{N_a} m_a (2\lambda_{na}) + \sum_{c=1}^{N_c} m_c (2\lambda_{nc}) + \sum_{c=1}^{N_c} \sum_{a=1}^{N_a} m_c m_a \zeta_{Nca} \quad \text{(A5)}$$

where F is given by:

$$F = -A^{\Phi} \left(\frac{\sqrt{I}}{1 + 1.2\sqrt{I}} + \frac{2}{1.2} ln(1 + 1.2\sqrt{I}) \right) + \sum_{c=1} \sum_{c'=c+1} m_c m_{c'} \Phi'_{cc'} + \sum_{a=1} \sum_{a'=a+1} m_a m_{a'} \Phi'_{aa'} + \sum_{c=1}^{N_c} \sum_{a=1}^{N_a} m_c m_a B'_{ca} \quad \text{(A6)}$$

C_{MX} is derived from C_{MX}^{Φ} as:

$$C_{MX} = \frac{C_{MX}^{\Phi}}{2\sqrt{|z_M z_X|}} \quad \text{(A7)}$$

and Z is calculated as:

$$Z = \sum_{k=1}^{N} |z_k| m_k \quad \text{(A8)}$$

The Pitzer virial coefficients, B_{MX}^{Φ}, B_{MX}, B'_{MX}, α_{MX}, C_{MX}, λ_{NC} and λ_{NA} in Equation (A2) through (A7) are described below.

B_{MX}^{Φ}, used to calculate the osmotic coefficient and water activity, is defined according to:

$$B_{MX}^{\Phi} = \beta_{MX}^{(0)} + \beta_{MX}^{(1)} e^{-\alpha_{MX}\sqrt{I}} + \beta_{MX}^{(2)} e^{-\alpha'_{MX}\sqrt{I}} \quad \text{(A9)}$$

where $\beta_{MX}^{(0)}$, $\beta_{MX}^{(1)}$, $\beta_{MX}^{(2)}$, and α_{MX} are temperature-dependent ion-interaction parameters.

B_{MX} is used to calculate the activity coefficient of charged species (ions). This coefficient is calculated as:

$$B_{MX} = \beta_{MX}^{(0)} + \beta_{MX}^{(1)} g(\alpha_{MX}\sqrt{I}) + \beta_{MX}^{(2)} g(\alpha_{MX}^{'}\sqrt{I}) \tag{A10}$$

with function g(x) defined as:

$$g(x) = 2(1-(1+x)e^{-x})/x^2 \tag{A11}$$

and x denoting $\alpha_{MX}\sqrt{I}$ or $\alpha_{MX}^{'}\sqrt{I}$, respectively.

$B_{MX}^{'}$ is used to calculate the modified Debye-Hückel term, and is formulated as:

$$\begin{aligned} B_{MX}^{'} &= \frac{\partial B_{MX}}{\partial I} \\ &= \beta_{MX}^{(1)} \frac{g'(\alpha_{MX}\sqrt{I})}{I} + \beta_{MX}^{(2)} \frac{g'(\alpha_{MX}^{'}\sqrt{I})}{I} \end{aligned} \tag{A12}$$

with function $g^{'}(x)$ defined as:

$$g'(x) = -2(1-(1+x+\frac{x^2}{2})e^{-x})/x^2 \tag{A13}$$

and x denoting $\alpha_{MX}\sqrt{I}$ or $\alpha_{MX}^{'}\sqrt{I}$, respectively.

For any salt containing a monovalent ion, α_{MX} = 2 and $\alpha_{MX}^{'}$ =12; for 2-2 electrolytes, α_{MX} = 1.4 and $\alpha_{MX}^{'}$ =12; for 3-2, 4-2, and higher valence electrolytes, α_{MX} = 2.0 and $\alpha_{MX}^{'}$ =50.

Note that Φ_{cc}^{ϕ}, Φ_{aa}^{ϕ}, Φ_{cc}, Φ_{aa}, $\Phi_{cc}^{'}$, $\Phi_{aa}^{'}$ are interaction parameters for like-sign ionic pairs (mixing terms). They are temperature and ionic strength dependent:

$$\Phi_{ij}^{\phi} = \theta_{ij} + {}^{E}\theta_{ij}(I) + I\,{}^{E}\theta_{ij}^{'}(I) \tag{A14}$$

$$\Phi_{ij} = \theta_{ij} + {}^{E}\theta_{ij}(I) \tag{A15}$$

$$\Phi_{ij}^{'} = {}^{E}\theta_{ij}^{'}(I) \tag{A16}$$

Terms ${}^{E}\theta_{ij}(I)$ and ${}^{E}\theta'_{ij}(I)$ are functions of the ionic charges between the pair and solution ionic strength. These functions are defined in Pitzer (1991) and can normally be ignored in moderately concentrated solutions of ionic strength less than 10 molal (for all like-sign pairs, ${}^{E}\theta_{ij}(I)=0$ and ${}^{E}\theta'_{ij}(I)=0$). Also, θ_{ij} are temperature-dependent fitting parameters, with ${}^{E}\theta_{ij}(I)$ and ${}^{E}\theta'_{ij}(I)$ calculated according to Pitzer (1991). Ψ_{cca} and Ψ_{caa} are the temperature dependent interaction coefficients of ternary terms. ζ_{nca} is the temperature dependent interaction coefficient of neutral-cation-anion terms. Normally, this term is ignored (for all neutral-cation-anion triplets, $\zeta=0$).

A.2 SIMPLIFICATIONS OF THE PIZER MODEL IMPLEMENTED IN TOUGHREACT

When the Pitzer model is used in geochemical simulations, the calculation of ionic interactions can be computationally intensive. For reactive transport problems, calculations of ionic interaction make the simulation intensive and time consuming. On the other hand, a complete expression of the Piztzer's ionic interaction theory would need infinite interaction terms in the virial equation. Any explicit expression of the model, including those in Pitzer's orginal formulations and the HMW model, is just a simplified representation of the Pitzer's ionic interaction theory. Different levels of simplifications can be applied to solutions with different levels of ionic strength, without significant loss of accuracy. These simplifications can reduce the computational resources requirement and lead to a significant computational time saving. TOUGHREACT provides four different levels of simplification based on the standard HMW model. If MOPR(22) and MOPR(23) are set to 0, TOUGHREACT runs a full implementation of the HMW model (Eqs. A1 though A16). Simplifications are performed by assigning non-zero values to MOPR(22) and MOPR(23) as described below.

A.2.1 Simplification 1, MOPR (23)=1

This setup neglects the ionic strength dependence of the mixing terms. With this setup, Equation (A14), (A15), and (A16) reduce to:

$$\Phi^{\phi}_{ij}=\theta_{ij} \tag{A17}$$

$$\Phi_{ij}=\theta_{ij} \tag{A18}$$

$$\Phi'_{ij}=0 \tag{A19}$$

No changes in other equations are made. This simplification is not recommended for use when dealing with solutions having an ionic strength higher than 10 molal.

A.2.2 Simplification 2, MOPR(22)=1

This setup neglects the neutral-cation-anion terms (the last term) in Equations (A2) and (A5). These equations are then reduced to:

$$\sum_{i=1}^{N} m_i(\phi-1) = 2(-\frac{A^{\Phi} I^{\frac{3}{2}}}{1+1.2\sqrt{I}}) + \sum_{c=1}^{N_c}\sum_{a=1}^{N_a} m_c m_a (B_{ca}^{\Phi} + ZC_{ca})$$
$$+ \sum_{c}\sum_{c'=c+1} m_c m_{c'} (\Phi_{cc'}^{\phi} + \sum_{a=1} m_a \psi_{cc'a})$$
$$+ \sum_{a}\sum_{a'=a+1} m_a m_{a'} (\Phi_{aa'}^{\phi} + \sum_{c=1} m_c \psi_{aa'c})$$
$$+ \sum_{n=1}^{N_n}\sum_{c=1}^{N_c} m_n m_c \lambda_{nc} + \sum_{n=1}^{N_n}\sum_{a=1}^{N_a} m_n m_a \lambda_{na} \quad \text{(A20)}$$

and

$$\ln \gamma_N = \sum_{a=1}^{N_a} m_a (2\lambda_{na}) + \sum_{c=1}^{N_c} m_c (2\lambda_{nc}) \quad \text{(A21)}$$

Other equations are unchanged. This simplification generally yields virtually the same results as the full formulations, because the neutral-cation-anion terms are typically insignificant. In addition, the parameters of these terms are usually not available, making the full formulation perform like the simplified formulation. Thus, this simplification can be used in most cases.

A.2.3 Simplification 3, MOPR(22)=2

In addition to the terms neglected in Simplification 2, this option neglects the cation-cation-anion and the cation-anion-anion terms in Equation (A2), (A3), and (A4). These equations then reduce to:

$$\sum_{i=1}^{N} m_i(\phi-1) = 2(-\frac{A^{\Phi} I^{\frac{3}{2}}}{1+1.2\sqrt{I}}) + \sum_{c=1}^{N_c}\sum_{a=1}^{N_a} m_c m_a (B_{ca}^{\Phi} + ZC_{ca})$$
$$+ \sum_{c}\sum_{c'=c+1} m_c m_{c'} \Phi_{cc'}^{\phi} + \sum_{a}\sum_{a'=a+1} m_a m_{a'} \Phi_{aa'}^{\phi} \quad \text{(A22)}$$
$$+ \sum_{n=1}^{N_n}\sum_{c=1}^{N_c} m_n m_c \lambda_{nc} + \sum_{n=1}^{N_n}\sum_{a=1}^{N_a} m_n m_a \lambda_{na}$$

$$\ln \gamma_M = Z_M^2 F + \sum_{a=1}^{N_a} m_a (2B_{Ma} + ZC_{Ma})$$
$$+ 2\sum_{c=1}^{N_c} m_c \Phi_{Mc} + |Z_M| \sum_{c=1}^{N_c}\sum_{a=1}^{N_a} m_c m_a C_{ca} + 2\sum_{n=1}^{N_n} m_n \lambda_{nM} \quad \text{(A23)}$$

$$\ln \gamma_X = Z_X^2 F + \sum_{c=1}^{N_c} m_c (2B_{cX} + ZC_{cX})$$
$$+ 2\sum_{c=1}^{N_c} m_a \Phi_{Xa} + |Z_x| \sum_{c=1}^{N_c}\sum_{a=1}^{N_a} m_c m_a C_{ca} + 2\sum_{n=1}^{N_n} m_n \lambda_{nX} \quad \text{(A24)}$$

This simplification can be generally used for solutions with an ionic strength smaller than about 10 molal.

A.2.4 Simplification 4, MOPR(22)=3

In addition to the terms neglected in Simplification 3, this setup neglects cation-cation and anion-anion terms in Equations (A2), (A3), and (A4), which reduce to:

$$\sum_{i=1}^{N} m_i(\phi - 1) = 2(-\frac{A^{\Phi} I^{\frac{3}{2}}}{1 + 1.2\sqrt{I}}) + \sum_{c=1}^{N_c}\sum_{a=1}^{N_a} m_c m_a (B_{ca}^{\Phi} + ZC_{ca}) + \sum_{n=1}^{N_n}\sum_{c=1}^{N_c} m_n m_c \lambda_{nc} + \sum_{n=1}^{N_n}\sum_{a=1}^{N_a} m_n m_a \lambda_{na} \quad \text{(A25)}$$

$$ln\gamma_M = Z_M^2 F + \sum_{a=1}^{N_a} m_a(2B_{Ma} + ZC_{Ma}) + |Z_M| \sum_{c=1}^{N_c}\sum_{a=1}^{N_a} m_c m_a C_{ca} + 2\sum_{n=1}^{N_n} m_n \lambda_{nM} \quad \text{(A26)}$$

$$ln\gamma_X = Z_X^2 F + \sum_{c=1}^{N_c} m_c(2B_{cX} + ZC_{cX}) + |Z_x| \sum_{c=1}^{N_c}\sum_{a=1}^{N_a} m_c m_a C_{ca} + 2\sum_{n=1}^{N_n} m_n \lambda_{nX} \quad \text{(A27)}$$

This simplification can be generally used for solutions with an ionic strength smaller than 5 molal.

Note that the use of the full version of the formulation (no simplification) usually yields better results if all interaction parameters are available and self-consistent; in this case, simplification is not encouraged if computational power is not limited. Note also that because interaction parameters are typically obtained by fitting experimental data using some level of simplification in the HMW formulation, the user should be careful to set a simplification level that matches (as well as possible) the formulation used to fit the experimental data.